PHASING A DUAL OPTICAL PATH SYSTEM USING AN
OPTICAL FIBER AS A PHASE CONJUGATE MIRROR

THESIS

Shawn M. Willis, 2Lt, USAF

AFIT/GAP/ENP/03-06

**DEPARTMENT OF THE AIR FORCE**
**AIR UNIVERSITY**

# AIR FORCE INSTITUTE OF TECHNOLOGY

**Wright-Patterson Air Force Base, Ohio**

AFIT/GAP/ENP/03-06

PHASING A DUAL OPTICAL PATH SYSTEM USING AN OPTICAL FIBER AS A

PHASE CONJUGATE MIRROR

THESIS

Presented to the Faculty

Graduate School of Engineering and Management

Air Force Institute of Technology

Air University

Air Education and Training Command

In Partial Fulfillment of the Requirements for the

Degree of Master of Science (Applied Physics)

Shawn M. Willis, BS

2Lt, USAF

March 2003

AFIT/GAP/ENP/03-06

PHASING A DUAL OPTICAL PATH SYSTEM USING AN OPTICAL FIBER AS A

PHASE CONJUGATE MIRROR

Shawn M. Willis, BS
2Lt, USAF

Approved:

| | |
|---|---|
| Won B. Roh (Chairman) | 3 Mar 03 |
| | date |
| Glen P. Perram (Member) | 3 MAR 03 |
| | date |
| Timothy H. Russell (Member) | 3 MAR 2003 |
| | date |

# Acknowledgments

I would first like to thank God for allowing me the opportunity to attend the Air Force Institute of Technology, and helping complete this project. In addition, there are a few individuals whose support throughout this project was invaluable, and need to be recognized. First, I would like to mention Dr. Won B. Roh. His guidance during the course of this project was a key element to the successful completion of this thesis. He was always available to give technical advice and guidance, but still allowed me to decide the direction of the investigations. His demeanor led to a relationship that was not only conducive to learning, but also a joy to work with. I would also like to thank Captain Timothy Russell for taking the time to teach me valuable laboratory skills, and for being available to answer questions. I also need to mention Dr. Sung H. Baek, and thank him for the valuable suggestions he gave me during the course of this project. More thanks go to the laboratory technicians: Greg Smith, Michael Ranft, and James Malone for help with some technical problems during this project. Another individual who needs to be mentioned is 2$^{nd}$ Lieutenant Matthew Crookston. The many discussions we had together allowed me to bounce ideas off him, and talk through the various difficulties I ran into. Finally, I had the support of my wife, whom without there is nothing. This is for her.

Shawn M. Willis

# Table of Contents

# List of Figures

# **Abstract**

Phase conjugation properties of stimulated Brillouin scattering (SBS) in a short multimode fiber have been investigated with an eye towards its application for a multi-channel double pass master oscillator power amplifier (MOPA) system. In particular, properties of the SBS beam to compensate for the axial and transverse phase distortion between individual channels in a multi-channel amplifier system were studied. Two optical paths were created by covering half of the laser beam with a microscope slide, and also by spatially splitting the wavefronts with a 4 prism set-up. The Stokes beams that traversed the same optical paths as the pump beams were shown to compensate the phase distortion introduced by the different optical paths.

**PHASING A DUAL OPTICAL PATH SYSTEM USING AN OPTICAL FIBER AS**

**A PHASE CONJUGATE MIRROR**

# 1  Introduction

## *1.1.        Motivation*

Laser devices have become common in our society, and are used in many different applications.  Examples range from the medical field where lasers are used to correct vision, the scientific research area where the OMEGA laser system is used to cause thermonuclear fusion, to the average household where lasers read compact discs to play music.[1]  Even with the advances that have already been made in the laser field, there is still much more to be gained.  The department of defense recognizes this, and has deemed laser systems to be critical to the modern military.[2]

A particular area of interest is high energy lasers.  One approach to achieving high energy lasers is to use amplifiers to increase the energy.  To increase the energy beyond the maximum level achieved with one amplifier, multiple amplifiers can be used in parallel.  Unfortunately, splitting the beam into multiple paths comes with a price.  When the beam is split and travels along separate optical paths, a phase delay known as a piston error is introduced between the beams.  Therefore, upon recombination of the beams, the wavefronts are no longer phased.  In order to correct for the piston errors that arise, a double-pass MOPA system which utilizes a phase conjugate mirror can be used instead of the single-pass MOPA system.

In a multi-channel double pass MOPA, the beams traveling separate paths are reflected and passed back through the amplifiers where they are finally recombined.  If a conventional mirror is used to reflect the beams, the piston errors become greater due to the beams traveling the separate paths twice.  On the other hand, if a phase conjugate mirror is used, the piston errors introduced from the first pass through the separate paths are eliminated when the beams travel back along their same paths.  An effective way to create a phase conjugate mirror which will eliminate the piston errors is through stimulated Brillouin scattering (SBS).[3]  In addition to eliminating the piston errors, SBS phase conjugation also provides a way to compensate for aberrations in the optical system.[4]

The advantage of phasing the output beams lies in the intensity of the far-field beam spot.  Due to diffraction, the far-field spot size of a beam is inversely proportional to the spot size of the output beam.  Therefore, a smaller output beam will have a larger far-field spot. In an N-channel MOPA system that has not been phased, the output consists of N independent output beams.  The far-field patterns of each beam overlap, yielding N times the intensity of a single beam.  When the N beams are phased, the output beam is a single larger beam, which leads to a smaller far-field spot.  The far-field intensity in this case is $N^2$ times the intensity of a single beam.

Experiments have been done to test the phasing ability of SBS phase conjugation in systems where the beam is forced to travel multiple paths.  This would be similar to a MOPA system without the amplifiers.  In 1988, Moyer and others demonstrated the phasing ability of SBS phase conjugation in a system where the beam traveled two separate paths.  The beams were focused into a methanol SBS cell in order to produce the SBS.[3]  A drawback when using SBS cells as a phase conjugate mirror is the small

2

tolerance for misalignment within the cell.  In order to obtain phase conjugation for both beams, they must to be focused into a common focal volume, which is a very difficult task.  Sternklar and others showed that when the plane of the beam paths is in the horizontal direction, slight vertical misalignment diminished the SBS output significantly.[5]

Another medium in which SBS can occur is optical fibers.  An interesting property of fibers is that the length of the fiber has a bearing on the characteristics of the SBS. In long multimode optical fibers, SBS generates a Stokes beam that propagates in the fiber $LP_{01}$ mode, making it good for beam cleanup.  An AFIT group showed that an aberrated pump beam coupled into a long multimode optical fiber generated a Gaussian-like Stokes beam.[6]  On the other hand, in short fibers the SBS produces a Stokes beam that is the phase conjugate of the input, or pump beam.[7]  It is this property that is useful for the MOPA system, and the motivation for this project.

## *1.2.        Overview*

The goal of this project was to investigate the phasing properties of the SBS from a short multimode optical fiber when the fiber was used as a phase conjugate mirror for a system in which the pump beam has been split into multiple paths and is recombined. Specifically, this investigation was oriented towards demonstrating the ability of SBS phase conjugation from the fiber to eliminate the piston errors introduced when one beam is split and forced to travel separate optical paths.

The first part of the investigation was to simply achieve phase conjugation using the optical fiber.  Phase conjugation was determined by how well the fiber could correct for phase distortions introduced by placing an aberrating medium in the beam path.  This

3

investigation was accomplished using two different aberrating mediums, a stretched piece of plastic and a -50 cm focal length lens. The investigation process is as follows. A laser beam was passed through the aberrating medium and then, either retro-reflected using a high reflector or coupled into an optical fiber to generate a backward traveling Stokes wave through SBS. The backward traveling beam, either a reflection or Stokes beam, passed back through the aberrator and the profile was recorded using a frame grabber. The beam profiles with the aberration medium in the beam path were compared with reference profiles which were created by removing the aberrating medium from the system. Since there was only a short amount of time to complete the project, a more rigorous analysis of the phase conjugate beam was not carried out.

Next, the first experiment to test the phasing ability of the SBS beam was carried out. Instead of using the aberrating medium as was done to test for phase conjugation, a microscope slide was placed over half of the beam creating two separate optical paths, one for each half of the pump beam wavefront. A lateral shearing interferometer was used to create an interferogram from the output beam that was recorded by the camera. The continuity or discontinuity of the interference fringes within the interferogram served as a test for phasing.

The final phasing experiment utilized a setup that more closely resembles that of a MOPA system. The beam wavefront was split into two different optical paths using prisms that guided the split beams in paths that were spatially apart from each other. An attempt to diagnose the output with the lateral shearing interferometer was made, but the results were not as clear as would be desired. Therefore, a different approach was used to determine the phasing ability of the fiber for this system. The lateral shearing interferometer was removed from the setup, and the output beam was viewed with the

4

CCD camera.  The beam profile was checked for the formation of interference fringes at the camera.  In a system where the beam wavefront is split and travels separate paths, phase errors arise between the beams.  If the phase errors are not compensated, the beam will not be phased when the paths are recombined, and interference fringes will be visible at that point.  On the other hand, if the phase errors are compensated, the recombined beams will be phased, and no interference fringes will be observed.  It was also necessary to demonstrate that the Stokes beams exiting the fiber were coherent, since if the Stokes beams were not coherent, no interference fringes would be observed at the camera. Therefore, in order to determine if the absence of interference fringes at the camera was due to phasing of the beams or lack of coherence between the beams, the Stokes beams were checked for coherence.  This was done by using the lateral shearing interferometer to overlap the separate beams immediately after they exited the fiber.  Interference fringes at this point demonstrated the beams were coherent.

Chapter 2 discusses the theory of phase conjugation, stimulated Brillouin scattering, and how these could be useful to a MOPA system.  The ability of a short fiber to produce a phase conjugated beam is examined in Chapter 3.  Chapter 4 describes the experimental work and results obtained when the microscope slide was used to create separate optical paths.  The experimental work and results when the prisms were used to create the optical paths is discussed in Chapter 5.  Chapter 6 examines the pulse width and energy response of the SBS beam.  Chapter 7 discusses the accidental damage that was done to the lens and the polarization of the SBS beam.  Final conclusions are made in Chapter 8.

# 2 Theory

## 2.1.        *Phase Conjugation*

Optical phase conjugation is a process in which the spatial portion of the phase factor of an arbitrary beam of light is exactly reversed.[8]   Figure 2.1 demonstrates the difference in propagation vectors between a phase conjugate reflector and a conventional mirror.  A conventional mirror reverses only the normal component of the propagation vector upon reflection, while leaving the tangential components unchanged.  This allows the reflected beam to be directed arbitrarily by simply adjusting the orientation of the mirror.  A phase conjugate mirror, on the other hand, reverses each component of the propagation vector.  This causes the light to be reflected exactly back upon itself, independent of the phase conjugate mirror's orientation.

(a)                                                           (b)



$$\bar{k}_{in} = k_x\hat{x} + k_y\hat{y} + k_z\hat{z}$$
$$\bar{k}_{out} = k_x\hat{x} + k_y\hat{y} - k_z\hat{z}$$

$$\bar{k}_{out} = -\bar{k}_{in}$$
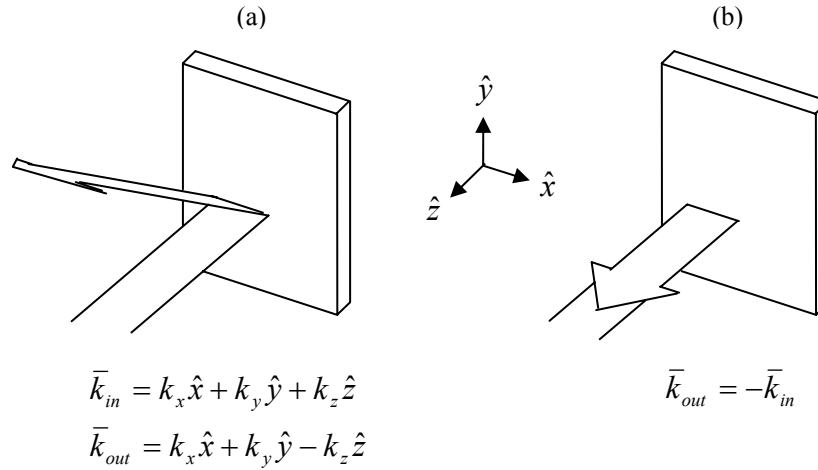
**Figure 2.1** Propagation vector reflections.

(a) The reflection from a conventional mirror reverses only the normal component of the propagation, leaving the tangential components unchanged. (b) The reflection from a phase conjugate mirror reverses each component of the propagation vector.

This phenomenon can be seen by considering the propagation of a

monochromatic wave along the positive z-direction. The wave can be represented by

$$\vec{E}_p(\vec{r},t) = \frac{1}{2}\vec{\varepsilon}_p(\vec{r})e^{i(\omega t - k_p z)} + c.c. \quad (2.1)$$

where

$\vec{\varepsilon}_p(\vec{r})$ = slowly varying, complex amplitude of the field

$\omega$ = angular frequency of the monochromatic wave

t = time

$k_p = \omega c/n$, wavevector magnitude (c = speed of light, n = refractive index)

c.c. = complex conjugate.

The slowly varying, complex amplitude contains not only spatial information of the field,

but it can also contain information about the polarization of the field.[9] The phase

conjugate wave corresponding to the monochromatic plane wave is simply the complex

conjugate of equation (2.1), which is given by

$$\vec{E}_c(\vec{r},t) = \frac{1}{2}\vec{\varepsilon}_c(\vec{r})e^{i(\omega t + k_p z)} + c.c. \quad (2.2)$$

where

$\vec{\varepsilon}_c = \vec{\varepsilon}_p^*$, complex conjugate of the slowly varying, complex amplitude.

The relationship between the two waves given by equations (2.1) and (2.2) is

$$\vec{E}_c(\vec{r},t) = \vec{E}_p(\vec{r},-t). \quad (2.3)$$

From this relation, it is seen that the phase conjugate wave propagates as if the input

wave were time reversed. In other words, the light retraces the exact path it followed to

reach the phase conjugation mirror. Therefore, the effect of a phase conjugate mirror is

to not only reverse the propagation, but to also invert the wavefronts of the incident wave with respect to the direction of propagation.[9] This means that in terms of the coordinate system, the phase conjugated wavefront has the same shape as the incident wavefront, since the direction of propagation reverses at the phase conjugate mirror.

These properties lead to many interesting applications. One such application is phase distortion correction. Figure 2.2 illustrates a plane wave passing through a phase-distorting medium followed by a reflection from either a conventional mirror or phase conjugating mirror.



Conventional mirror        Phase-conjugate mirror

Glass        Glass

(a)        (b)
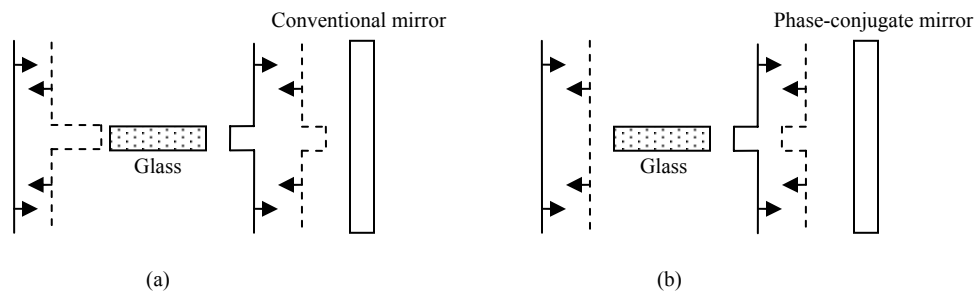
**Figure 2.2** Phase distortion correction.

(a) The reflection from a conventional mirror causes the wave plane to be reversed, so that upon passing through a phase distorting medium again, the phase delay is doubled. (b) The reflection from a phase-conjugate mirror does not reverse the wave plane. Therefore, a second pass through the phase distorting medium corrects the phase delay.

The incident wave passes through the phase distortion medium, in this case glass, and experiences a phase delay. The reflection from a conventional mirror experiences a wave plane reversal in the coordinate system, so that when the light passes through the glass a second time, the phase delay is doubled. On the other hand, the reflection from the phase-conjugate mirror only experiences a propagation reversal, leaving the shape unchanged in the coordinate system. Therefore, when the light passes back through the

8

glass, the phase delay is compensated for and the wavefront has the same shape as the incident wavefront.[10]

It also follows from the characteristics of a phase-conjugated wave that a phase conjugate mirror can be used to restore aberrated wavefronts to their initial states. Figure 2.3 shows an incident plane wave passing through a linear aberrator resulting in distorted equiphase surfaces. The linear aberrator is a linear, lossless, inhomogeneous spatially dependent phase aberrating medium. After the reflection from the phase conjugate mirror, the distorted wave passes back through the aberrator and the initial planar equiphase surfaces are recovered.[9]
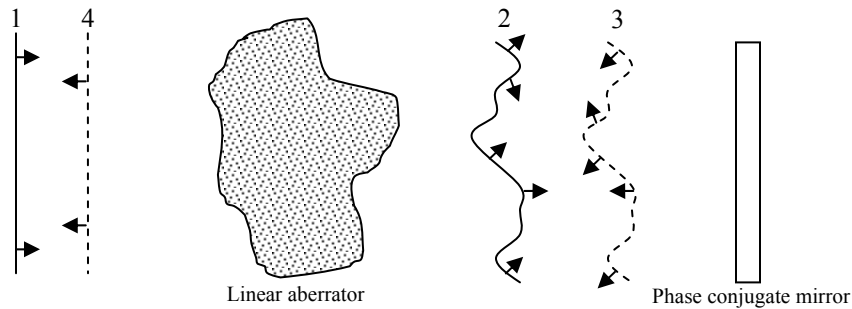


**Figure 2.3** Wavefront restoration.

A monochromatic plane wave (1) passes through a linear aberrator and becomes distorted (2). The distorted wavefront is phase conjugated (3) by the phase conjugate mirror, and passes back through the linear aberrator. The wave emerges from the aberrating medium with the same wavefront as the incident wave (4).

## 2.2.    *Stimulated Brillouin Scattering*

In optical media there is generally always a spontaneous acoustic wave field which is created by the thermal elastic motion of the particles making up the medium. If the thermal acoustic field is thought of as the superposition of monochromatic plane acoustic waves, then each of the acoustic waves can produce a periodic spatial and

temporal modulation of the density within the medium. This in turn creates an index

grating within the medium.[11]   For example, Figure 2.4 shows the displacement of

molecules within the medium in one dimension along with the index variation that is

created by the motion of the particles. When light is incident upon the medium, Brillouin

scattering, which results from the interaction between the incident optical wave and the

elastic acoustic waves in the optical medium, can occur.[11]
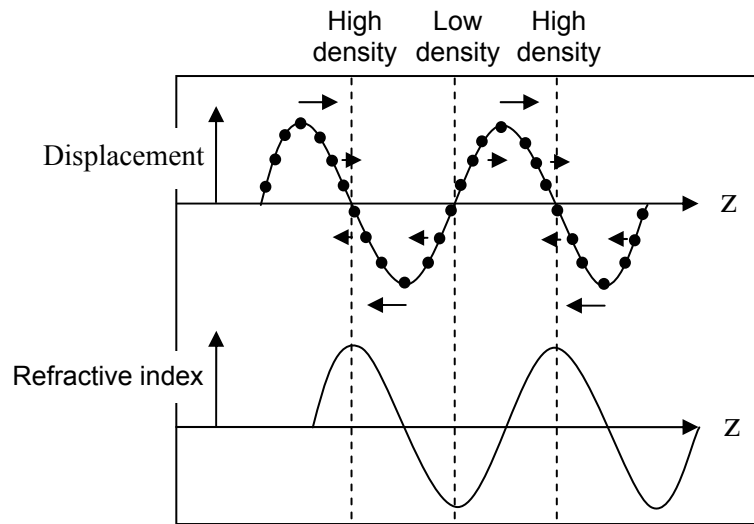


**Figure 2.4** Density and index variations within an optical medium.

The symmetric stretch vibration in one dimension produces regions of high and low densities. The regions
of high density correspond to regions of high refractive indices, while the regions of low density
correspond to regions of low refractive indices.

Now, the acoustic wavefronts are moving within the optical medium, which

causes the index grating to move. The incident light that is scattered off of the moving

index grating will therefore experience a frequency shift. For example, let the acoustic

wave be of frequency $\omega_a$ and the incident light be of frequency $\omega_L$. Also, let the acoustic

wavefronts be moving away from the incident light wave. The scattered light will then

be shifted downward in frequency to what is known as the Stokes frequency, which is

simply $\omega_s = \omega_L - \omega_a$. The down shift in frequency is due to the Doppler shift associated with a grating moving with the acoustic velocity $v_a$.[12] This process is depicted in Figure 2.5, and is a classical picture of spontaneous Brillouin scattering of light. In an ordinary medium, the thermal elastic field is very weak, and therefore the observation of Brillouin scattering from a conventional light source is difficult.[11]
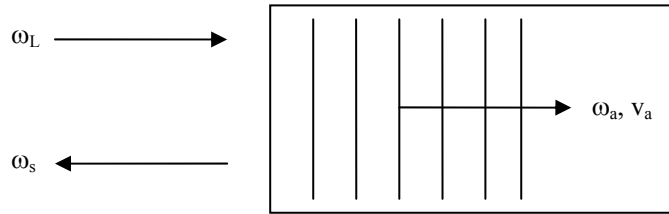


**Figure 2.5** Brillouin scattering.

An incoming wave with frequency, $\omega_L$, is incident on a grating moving with acoustic velocity, $v_a$, and frequency, $\omega_a$. The result is a Stokes wave with frequency, $\omega_s$, such that $\omega_s = \omega_L - \omega_a$.

By using a laser as the incident light source, it is possible that the interaction between the incident optical wave and the elastic acoustic wave can lead to stimulated Brillouin scattering (SBS). For this to occur, the interference of the laser field and the Stokes field must contain a frequency component equal to the acoustic field, $\omega_a$, within the medium. This begins a cyclic process in which the interference term of the laser and Stokes fields acts as a source that increases the amplitude of the acoustic field. This in turn increases the beating of the acoustic field and the laser field, which increases the Stokes field and therefore the beating of the laser and Stokes fields. The process continues to cycle through, and under the proper circumstances, leads to exponential growth of the amplitude of the Stokes wave.[13]

There are two physical mechanisms that cause the interference of the laser and Stokes waves to drive the acoustic wave. One of these mechanisms is optical absorption. This happens when the heat created by absorption in regions of high optical intensity causes the material to expand in those regions. SBS due to absorption is not commonly used since it only occurs in lossy material.[13] Therefore, optical absorption will not be discussed here. The other mechanism, known as electrostriction, is the tendency of materials to become more dense in regions of high optical intensity.[13]

As mentioned previously, the spontaneous Brillouin scattered light using a conventional light source is very weak. But, by using a laser of sufficient intensity as the incident light source, the spontaneously scattered light can become rather intense. Once this occurs, the incident and scattered light fields are able to beat together. It is at this point that electrostriction plays a role, and gives rise to density and pressure variations. The refractive index variations that follow from the density variations scatter the incident laser field such that the scattered light is at the Stokes frequency. This light is then able to add constructively with the Stokes radiation that initially gave rise to the acoustic disturbance. The acoustic and Stokes waves continue to reinforce each others growth, so that each can grow to large amplitudes.[13]

Since both the optical field and the acoustical field can be quantized, SBS can be described using a quantum theoretical model. When described in this manner, the Brillouin scattering process can be thought of as a parametric interaction between an input photon, a scattered photon, and a phonon within the medium.[11] The input photon acts as a pump photon, and will therefore be referred to as a pump photon. During the process the pump photon is annihilated, while simultaneously a scattered photon and

12

induced phonon are created. The process must conserve both momentum and energy. Therefore, the following equations must be true.

$$v_p = v_s + v_a \tag{2.4}$$

$$\bar{k}_p = \bar{k}_s + \bar{k}_a \tag{2.5}$$

where $v_p$, $v_s$, and $v_a$ are the frequencies of the pump photon, scattered photon, and induced phonon, and $k_p$, $k_s$, and $k_a$ are the wave vectors of the three quantities respectively.[11]

In the case of SBS, the acoustic phonon frequency is much smaller than the Stokes frequency. Therefore the acoustic phonon frequency can be neglected. This leads to the relationship given by

$$v_p \cong v_s . \tag{2.6}$$

This in turn, implies

$$\left|\bar{k}_s\right| \cong \left|\bar{k}_p\right|, \tag{2.7}$$

which leads to

$$\left|\bar{k}_a\right| \cong 2\left|\bar{k}_p\right|. \tag{2.8}$$

This can relationship can be seen in Figure 2.6.
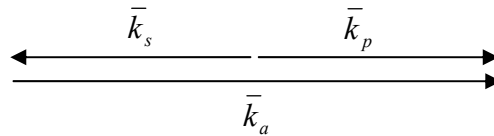


**Figure 2.6** SBS momentum vector diagram.

The acoustic phonon and pump photon momentum vectors are in the same direction, while the Stokes and pump photon momentum vectors are approximately equal in magnitude.

13

Therefore the following relationship can be written.

$$\frac{\omega_a}{v_a} = 2\frac{\omega_p}{c/n_p} \qquad (2.9)$$

where,

$\omega_a$ = angular frequency of the acoustic phonon

$v_a$ = velocity of sound in the medium

$\omega_p$ = angular frequency of the pump photon

$n_p$ = index of refraction of the medium at $\omega_p$

$c$ = speed of light in a vacuum.

Now using the relationship

$$\omega = 2\pi\upsilon \qquad (2.10)$$

where

$\omega$ = angular frequency

$\upsilon$ = frequency,

Equation 2.10 can be rewritten as

$$\frac{\upsilon_a}{v_a} = \frac{2\upsilon_p n_p}{c} \qquad (2.11)$$

where

$\upsilon_a$ = acoustic phonon frequency

$\upsilon_p$ = pump photon frequency.

Finally, the acoustic phonon frequency is given to be

14

$$\upsilon_a = 2\frac{\text{v}_a n_p}{c}\upsilon_p.$$  (2.12)

A phenomenon critical to this project is the ability of SBS to generate a Stokes beam that is the phase conjugate of the pump beam.[13] The Stokes beam does not have an absolute temporal reference though, and therefore the absolute phase factor is random.[15] This causes beams conjugated by SBS in separate interaction volumes to have a random phase difference. Therefore, it is necessary to overlap the beams in a common interaction volume to avoid the introduction of a random phase error between the beams.

In Moyer's investigation, SBS from a methanol cell was shown to have the ability to remove the piston errors caused by two beams traveling separate optical paths.[3] However, there are limitations on how much the path length can differ. First, the total path length difference must be a small fraction of the coherence length of the beams. The second limitation relates the SBS frequency shift to the total path length difference.[3, 14] For a given pump frequency and nonlinear medium, Equation 2.4 and Equation 2.5 determine the SBS frequency shift, which is simply the induced phonon frequency. The relationship between the total path length difference and the SBS frequency shift is then given by[3, 15]

$$\delta = \Delta_B \Delta L$$  (2.13)

where

$\delta$ = residual piston error due to path length difference

$\Delta L$ = total path difference between the beams in [cm],

and

$$\Delta_B = \frac{\Delta\upsilon_a}{c}, \quad \text{the SBS shift in } [\text{cm}^{-1}] \qquad\qquad (2.14)$$

where

$\Delta\upsilon_a$ = SBS frequency shift in [Hz].

For example, if a fiber is used with a pump beam at 1.06 μm, and not more than 0.1 wave phase difference is desired, $\Delta\upsilon_a$ = 16 GHz. This in turn corresponds to a maximum path length difference of 0.19 cm.

Stimulated Brillouin scattering in multi mode optical fibers has two important properties, one of which is essential to this project, that need to be mentioned. The first property is the ability of SBS to excite an $LP_{01}$ fiber mode even when an aberrated pump beam is used. This occurs only when the fiber is sufficiently long.[6] It is believed that this phenomenon occurs because the fundamental fiber mode experiences a higher gain relative to the higher-order modes when a multimode pump is used.[6] The application of this property lies in cleaning up aberrated beams. This project did not investigate beam clean up in this manner, and therefore further discussion of exciting an $LP_{01}$ fiber mode is not included in this paper. For more information on this topic see the reference from Rodgers.[6]

The property that is of interest to this project is the ability of SBS in multimode fibers to produce the phase conjugate wave of the incident beam. While phase conjugation from SBS does not occur in fibers only, the project here used a multi mode optical fiber to produce SBS. It is important to use a short fiber to observe phase conjugation from the SBS, and the maximum length of the fiber is given by different estimates from different authors. One of the expressions for the maximum length is given by[7]

$$L \leq \frac{6r_0^{\frac{1}{2}} c \pi^2}{\Delta \omega (NA)^2}$$

(2.15)

where

L = maximum allowable length

$r_0$ = allowable non-phase-conjugate fraction

c = speed of light

NA = numerical aperture of the fiber

and

$$\Delta \omega = \frac{4 \pi n}{\lambda_p} v$$

(2.16)

where

n = refractive index of the fiber core

v = velocity of sound in the medium

$\lambda_p$ = pump wavelength.

For example, the frequency shift, $\Delta v$, of SBS in a fiber is approximately 16 GHz, which corresponds to an angular frequency shift of $\Delta \omega = 10^{11}$. Using this value for $\Delta \omega$ and if $r_0 = 0.1$ and NA = 0.2, then the fiber should be no longer than 1.4 m. On the other hand, another author gives the maximum fiber length as[7, 16]

$$L \leq \frac{10Mc}{\Delta \omega (NA)^2}$$

(2.17)

where

M = coefficient dependent on pump power mode distribution.

The coefficient, M, has an order of magnitude of approximately 10, which would give an allowable fiber length of more than 10 times the amount of Equation 2.15 for the given

17

example.  Therefore, the equations should be taken as a reference which gives an

approximate order of magnitude.[7]

## 2.3.     *Applications to MOPA systems*

The conceptual design of a phase conjugate double-pass MOPA is shown in

Figure 2.7.
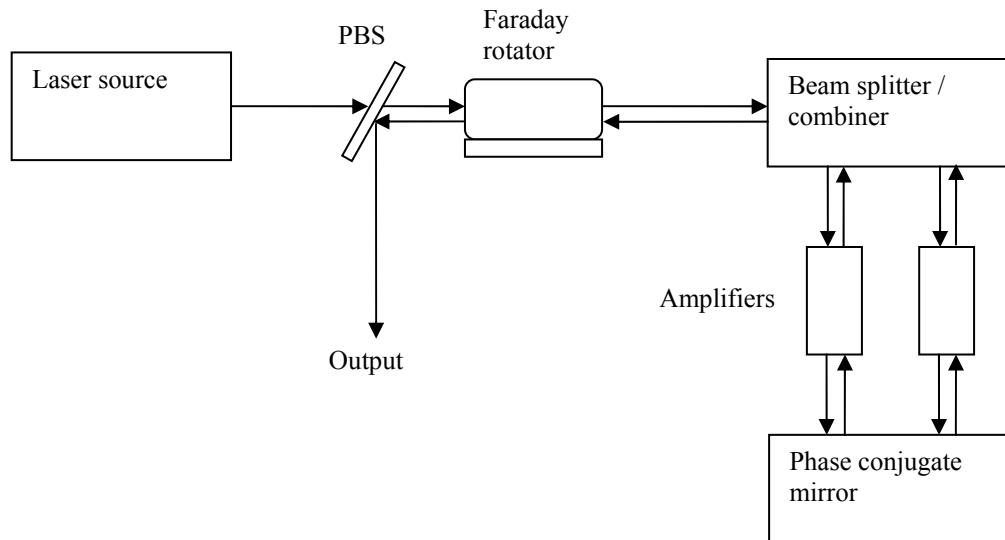
**Figure 2.7** Basic block diagram of a MOPA system.

A laser source produces a linearly polarized input beam for the system.  The beam travels

through a polarizing beam splitter, which is necessary in order to pick off the output

beam.  Next, the beam passes through a Faraday rotator, which rotates the polarization

orientation of the beam by $45^0$.  The beam is then split into multiple paths, and each beam

is amplified in an amplifier.  The beams from the amplifiers are combined and focused

18

into a multimode fiber, which serves as a phase conjugate mirror. The reflection from the phase conjugate mirror passes back through the amplifiers, where more amplification takes place, and into the Faraday rotator. The Faraday rotator rotates the polarization of the beam by another $45^0$, such that the polarization is rotated $90^0$ from the input beam. Now when the beam hits the polarizing beam splitter, it is reflected instead of transmitted due to the polarization rotation.

In general, when a beam is split into multiple paths and recombined, a phase delay (piston error) is introduced between the beams.[3] This is the reason for the phase conjugate mirror instead of a conventional mirror in the block diagram. As discussed in the phase conjugation section of this chapter, a phase conjugate mirror has the ability to eliminate the piston error that is introduced from the multiple paths.

Stimulated Brillouin scattering is a way to achieve phase conjugation, and one way to generate SBS is through the use of a short multi mode optical fiber. By coupling the beams from the multiple paths into the fiber, SBS occurs which produces phase conjugate beams. The beams must be coupled into a single fiber in order to avoid introducing a random absolute phase error between the beams. These beams travel back through the separate paths and the piston errors are eliminated due to the properties of phase conjugation.

# 3  Beam Phase Restoration through Phase Conjugation

The first step in this investigation was to show that the SBS from a short fiber is the phase conjugate of the incident light.  Due to time constraints, rigorous analysis of the SBS for phase conjugation was not performed.  Instead, the beam profiles of the SBS and retro-reflected beams were compared with and without a distortion medium present in the beam path.  This chapter first discusses the procedures in which the phase conjugation tests were conducted, and then discusses the results of the tests.

## *3.1.*     *Experimental Procedure*

The experimental set-up to show that the SBS from a short fiber is the phase conjugate of the incident beam is shown in Figure 3.1.
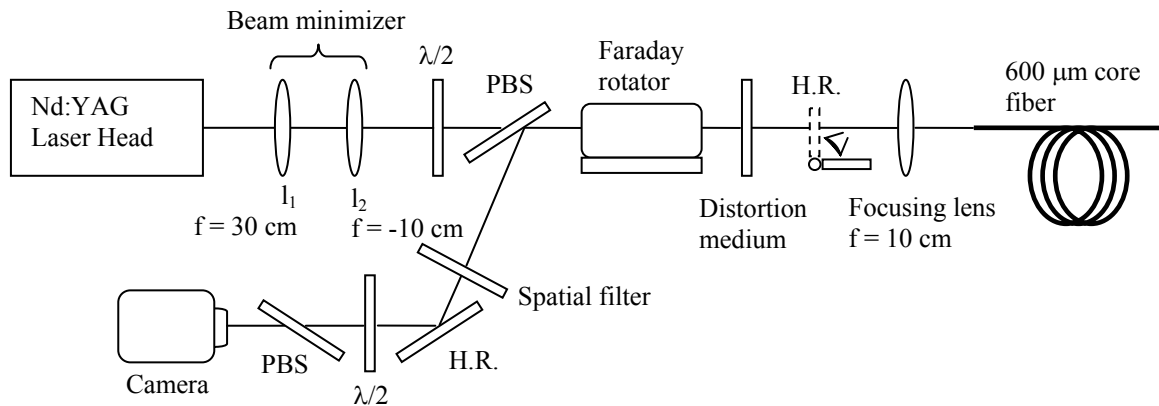


**Figure 3.1** Phase conjugation test set-up.

An injection seeded, Q-switched single-mode Nd:YAG laser was used to produce periodic 15 ns wide pulses at 30 Hz.  The light was linearly polarized at the output of the

laser.  Following the laser, the beam entered a telescope consisting of two lenses, with the first lens having a focal length of 30 cm, and the second lens having a focal length of -10 cm.  The telescope was used to reduce the beam size to match the aperture diameter of the Faraday rotator which formed a limiting factor for the diameter of the beam.  The beam emerging from the minimizing system had a diameter of approximately 4 mm.

Next, the beam passed through a half wave plate and polarizing beam splitter which, together, controlled the amount of light passed to the rest of the system.  The beam then entered a Faraday rotator, which rotates linearly polarized light by 45 degrees.  The direction of rotation is always the same regardless of which way the light travels through the Faraday rotator.  Following the Faraday rotator, the beam passed through an aberration medium.  Two different aberration media were used in this test.  The first one was a tightly stretched piece of plastic, and the second was a -50 cm focal length lens.  In order to take reference beam profiles to compare with the distorted beam profiles, the distortion medium was removed.

Following the aberrator, the beam was either retro-reflected by a high reflector or coupled into the 3.5 meter long 600 $\mu$m core diameter fiber with a numerical aperture of 0.37.  For the case when the fiber was used, a lens with a focal length of 10 cm was used to couple the beam into the fiber.  The return beam, whether it be the retro-reflection from the high reflector or SBS from the fiber, passes back through the distortion medium and the Faraday rotator.  At this point the polarization of the light has been rotated $90^0$ from the original polarization.  Therefore, it is now reflected at the polarizing beam splitter, instead of being transmitted.

The polarizing beam splitter was designed to be used in one direction.  As a result of using the return reflection from the polarizing beam splitter, three beam spots were observed instead of one.  A possible source of the extra spots is reflections from the back surface of the polarizing beam splitter.  In order to remove the extra spots, an adjustable aperture was placed in the beam path to act as a spatial filter which passed only the central spot.

Next, the beam was reflected off of a high reflector, and passed through a half wave plate and polarizing beam splitter.  Again, the half wave and polarizing beam splitter were used to control the amount of light passed to the rest of the set-up.  This was necessary because of the sensitivity of the CCD camera.  Finally, the beam was captured using a CCD camera. Beamcode, which is a frame grabber, was used to record the images.

## 3.2.      *Results*

Figure 3.2 shows the reference beam profiles using the high reflector as a retro-reflecting mirror and using the fiber to produce SBS viewed by the CCD camera without any distortion medium in the beam path.
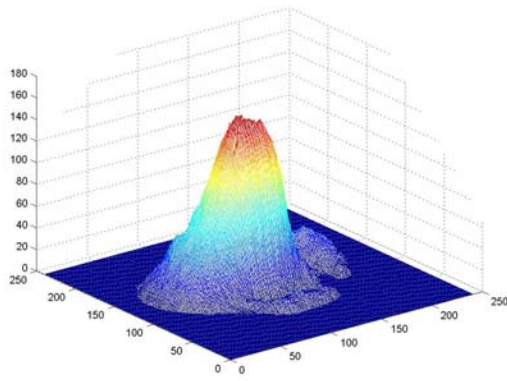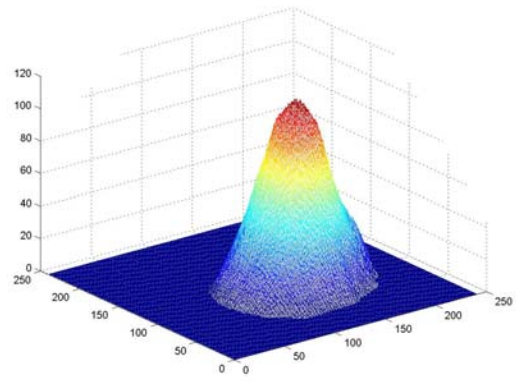
(a)                                                    (b)

**Figure 3.2** Beam profile references.

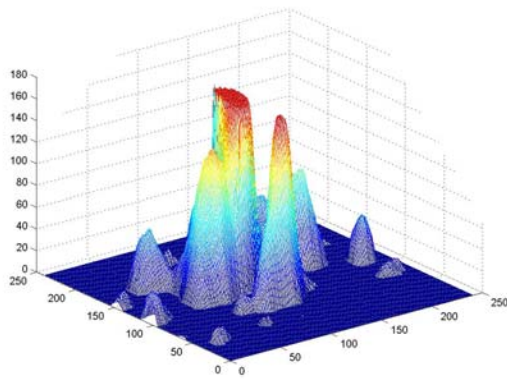(a) The beam profile viewed by the camera without any distortion medium in the beam path using the high reflector as a retro-reflecting mirror. (b) The beam profile viewed by the camera without any distortion medium in the beam path using the fiber to produce SBS.

In comparison, Figure 3.3 shows the beam profiles when a stretched piece of plastic, used as a distortion medium, was placed in the beam path as shown in Figure 3.1.
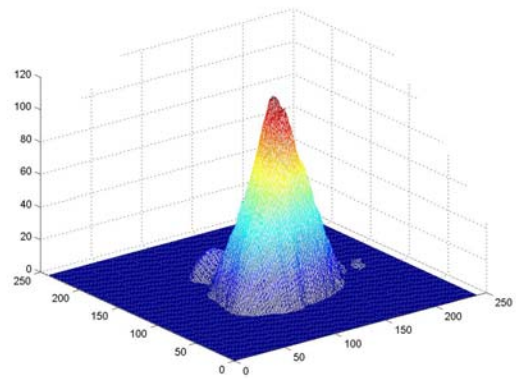


(a)                                                    (b)

**Figure 3.3** Beam profiles with a stretched piece of plastic in the beam path.

(a) The beam profile viewed by the camera using the high reflector as a retro-reflecting mirror with a stretched piece of plastic acting as the distortion medium in the beam path. (b) The beam profile viewed by the camera using the fiber to produce SBS with a stretched piece of plastic acting as the distortion medium in the beam path.

Comparison of Figure 3.2 (a) and Figure 3.3 (a) shows the distortion that is created by the plastic. The high reflector is a conventional mirror and does not posses any phase conjugation properties. Therefore, the distortion that is introduced on the first pass through the plastic is not corrected during the second pass through the plastic. Instead, the distortion is increased during the second pass. On the other hand, when the fiber is used instead of the high reflector, most of the distortion caused by the plastic is corrected during the second pass through the plastic. This can be seen by comparing the beam profiles of Figure 3.2 (b) and Figure 3.3 (b).

When the beam passes through the plastic, some of the light is lost due to scattering. This light never enters the fiber, and therefore does not pass back through the plastic. This explains the slight differences in beam profiles for the fiber with and without the plastic in the beam.

The same test was also conducted using a -50 cm focal length lens as the aberrator. Figure 3.4 demonstrates the results were similar to those obtained when the stretched plastic was used as the aberrator. The beam profiles without any distortion media present are shown in Figure 3.4 (a) and (b), while the beam profiles with the -50 cm focal length lens in the beam path are shown in Figure 3.4 (c) and (d). Comparisons of the corresponding beam profiles with and without the aberrator clearly demonstrate phase conjugation for the case when the fiber is used. The beam profile comparisons were enough to demonstrate phase conjugation for this project. The ability of the SBS generated Stokes beam to correct for the distortion introduced into the system is a good indicator of phase conjugation.

(a)

(b)
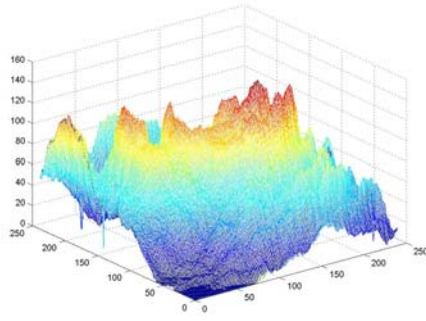
(c)
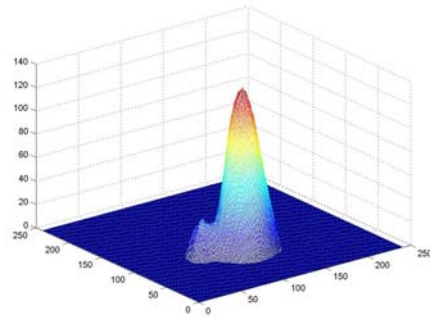
(d)

**Figure 3.4** Beam profile comparison with a -50 cm focal length lens aberrator
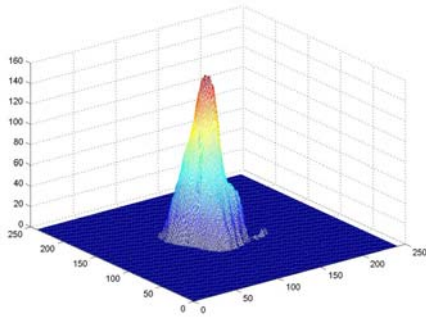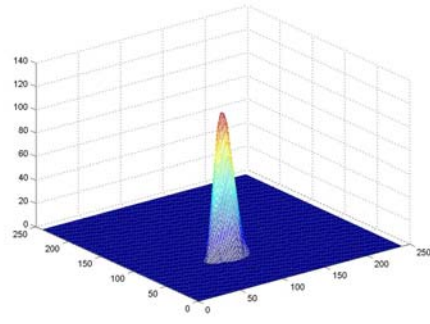
(a) The beam profile without any distortion media in the beam path using the high reflector as a retro-reflecting mirror. (b) The beam profile without any media in the beam path using the fiber to produce SBS. (c) The beam profile using the high reflector with a -50 cm focal length lens as the distortion medium in the beam path. (d) The beam profile using the fiber with a -50 cm focal length lens as the distortion medium in the beam path.

# 4  Wavefront Splitting Using a Microscope Slide

In order to demonstrate the phasing property of the phase conjugate Stokes beam, the pump beam wavefront was split into two halves, and one half was made to traverse a microscope. The splitting was accomplished by covering half of the beam with a microscope slide. The two halves were both focused into a single 600 μm core diameter fiber. In this way, each half traversed separate paths on their way to the fiber. After being coupled into the fiber, the generated Stokes beam passed back through the microscope slide where it was checked to see if phasing of the separate beam paths had occurred. This chapter first discusses the experimental procedures in which this test was carried out, and then delves into the results that were obtained from the experiment.

## *4.1.* *Experimental Procedure*

Figure 4.1 shows the experimental set-up to demonstrate phasing of a beam whose wavefronts are split by a microscope slide. The set-up is the same as the set-up shown in Figure 3.1, with two differences. The first difference is the replacement of the distortion medium with a microscope slide. The slide was mounted on a translational stage that allowed the slide to be positioned over half of the beam. In this way, the two optical paths were created. One path was through the microscope slide, while the other path was through the air. While this set-up would not allow the placement of amplifiers in the different optical paths, it was a good initial test to see if phasing of the separate beams would occur when using the fiber to get SBS.
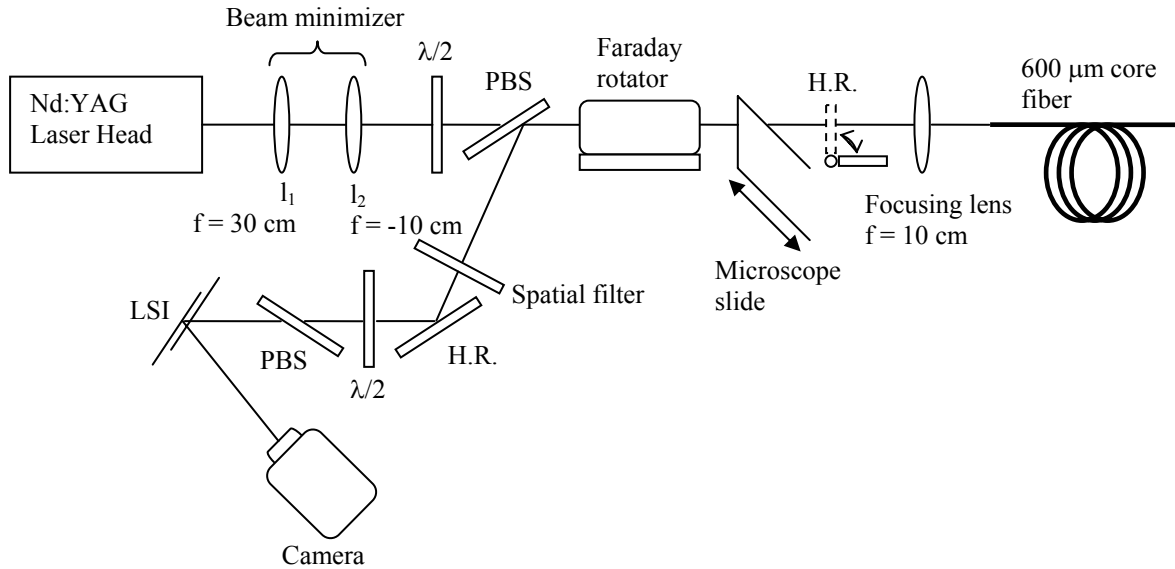
**Figure 4.1** Experimental set-up when splitting the wavefronts with a microscope slide.

The other difference is the use of a lateral shearing interferometer (LSI) before the camera. For information on the construction and operating theory of the LSI see Appendix A. Figure 4.2 shows three regions of interference in the reflection from the LSI. The fringe region on the left is the interference of beam 2 with its laterally displaced self, the fringe region in the middle is the interference of beam 1 with beam 2, and the fringe region on the left is the interference of beam 1 with itself. Continuity of the fringes across the three regions indicates compensation of the relative piston error between the beams.[3]

The interferogram created by the LSI reflection is then recorded by the camera. Once the interferograms are recorded, they can be investigated to determine if phasing of the two beams took place.
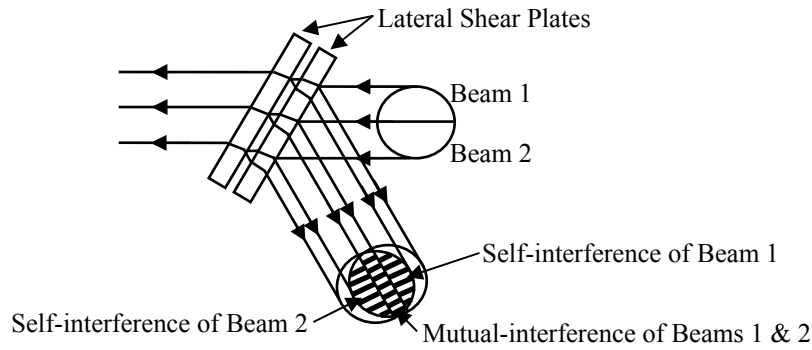
**Figure 4.2** Lateral shearing interferometer schematic.

Determining the boundary between the two beams proved to be difficult, so a thin strip of paper, approximately 1 mm wide, was placed over the edge of the microscope slide. This allowed there to be a greater separation of the two beams since the light incident on the paper was not transmitted. Figure 4.3 shows the beam incident on the slide and paper strip, and also, the resulting beam profile after passing the slide.
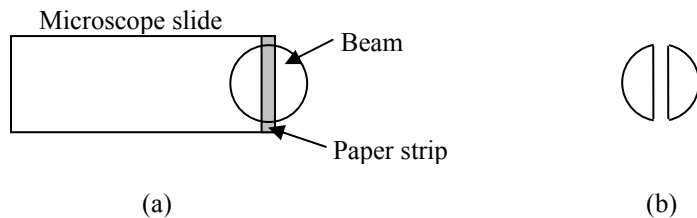


**Figure 4.3** Beam profile using a microscope slide to split the beam.

(a) Microscope slide covering half of the beam. The strip of paper allowed a greater distinction between the two separate optical paths. (b) Resulting beam profile when the 1 mm wide strip of paper was attached to the microscope slide.

## 4.2.    *Results*

The main diagnostic tool for this test was the LSI.  Figure 4.4 shows a comparison of the fringe patterns created by the LSI when the high reflector was used to retro-reflect the beam, and when the fiber was used to create SBS.
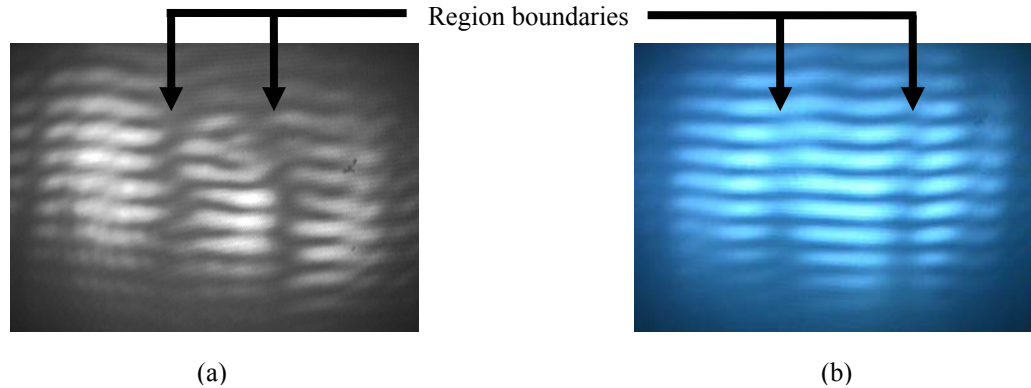


**Figure 4.4** Fringe regions from the LSI when a slide splits the beam.

(a) The fringe pattern from the LSI when the high reflector retro-reflected the beam. The discontinuity of the fringes at the boundaries indicates that conjugation of the relative piston errors between the two beams did not occur. (b) The fringe pattern from the LSI when the fiber caused SBS. The continuity of the fringes at the boundaries indicates conjugation of the relative piston errors between the two beams did occur.

The fringe pattern in Figure 4.4 (a) shows the three regions of interference when the high reflector is used to retro-reflect the beam.  As shown in the figure, the fringes are not continuous across the boundaries.  This indicates that compensation of the relative piston error between the beams traveling different optical paths does not occur.  On the other hand, the fringes in Figure 4.4 (b) are continuous across the boundary regions, and therefore indicate compensation of the relative piston errors.  The fringe pattern in Figure 4.4 (b) is for the case when the fiber is used instead of the high reflector.

By adjusting the LSI, the number of fringes could be controlled.  Figure 4.5 shows another set of fringe patterns resulting from splitting the beam wavefronts with the

microscope slide.  The fringes in this instance are wider, and the continuity or

discontinuity, depending on whether the fiber or high reflector was used, at the

boundaries is easily observed.  Again, it is shown that conjugation of the relative piston

error occurs for the case when the fiber is used, and does not occur when the high

reflector is used.



(a)                                                              (b)
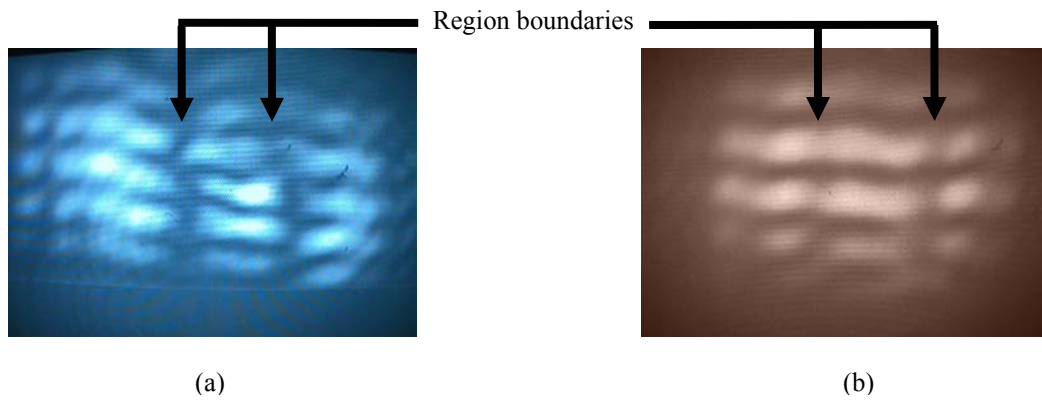
**Figure 4.5** Wide fringe patterns from the LSI when the beam is split by the slide.

(a) The fringe pattern when the high reflector is used. As in Figure 4.4 (a), there is discontinuity across the boundary regions. (b) The fringe pattern when the fiber is used. As is Figure 4.4 (b), there is continuity across the boundary regions.

# 5  Wavefront Splitting Using Four Prisms

After creating two optical paths by simply covering half of the beam with a microscope slide, the separate optical paths were created using 4 prisms to split the beam into separate paths, as shown in Figure 5.1.
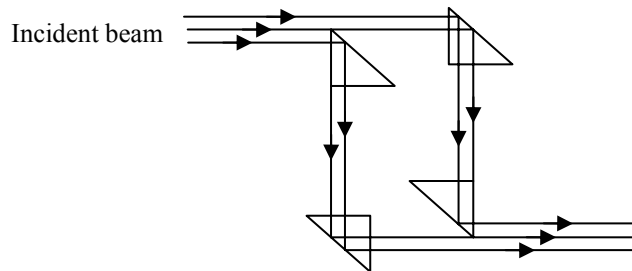


**Figure 5.1** Wavefront splitting using 4 prisms.

Half of the beam is incident on the edge of the first prism causing the two halves of the beam to travel separate paths. After each half of the beam traverses through two prisms the beam is recombined.

Splitting the beam in this manner is more meaningful than splitting the beam by simply covering half of the beam with a slide, since an actual MOPA system would require the spatial separation this configuration gives in order to place amplifiers in each leg.

During the course of this test, some interesting obstacles were encountered. The first of these was damaging the first lens in the beam minimizer lens combination. This is only noted in this chapter by a few changes in the experimental set-up. A discussion of this problem and the possible cause of this problem is carried out in Chapter 7. Another difficulty arose while trying to get well defined fringe patterns using the LSI. Due to some ambiguity, another test was also done to verify that phasing of the two optical paths was achieved.

Except for a few changes to the set-up that are described in the experimental procedures section of this chapter, the test to demonstrate phasing of the two beams using the LSI was carried out in the same manner as it was in Chapter 4. The results of that experiment were not as conclusive as those in Chapter 4, so as previously mentioned, another test was carried out.

To demonstrate the phasing property of the Stokes beams, the LSI was removed and replaced by a camera. The separate paths taken by the beams introduce a relative phase difference between the beams. If phasing does not occur, then the two beams will be out of phase at the camera, and interference fringes should be visible. On the other hand, if phasing does occur, then the beams should be in phase, and hence, no interference fringes should be visible. The absence of fringes by itself is not enough to demonstrate phasing though. The beams must also be shown to be spatially coherent, because incoherent beams would not produce interference fringes either. Therefore, the Stokes beam was picked off immediately upon passing back through the fiber coupling lens using the reflections off a pair of microscope slides. This reflection was then checked to see if the two beams were coherent, by looking for interference fringes. At this point, the two beams should not be completely phased since they have not returned through the prisms. By overlapping the reflections of beam 1 and beam 2, coherence can be checked by the presence or absence of interference fringes.

## *5.1.*        *Experimental Procedure*

Since two separate tests were completed to determine the phasing property of the

Stokes beam when the prisms were used to split the beam wavefronts, the experimental

procedure section of this chapter is divided into two sections.

### 5.1.1.        Phasing Test using the LSI

Figure 5.2 shows the set-up to test for phasing of the beams traveling different

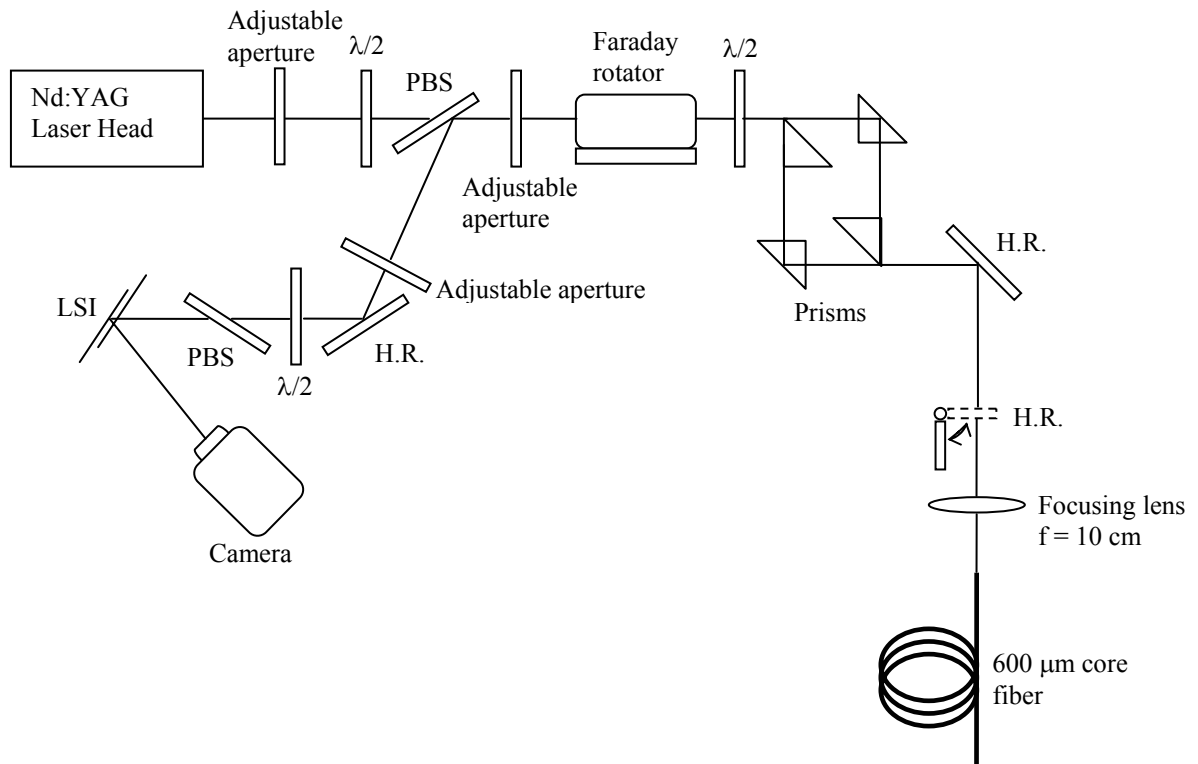paths through the prisms using the LSI method.



**Figure 5.2** Experimental set-up when splitting the wavefronts with prisms.

Instead of passing through a beam minimizing system (as was done previously), the diameter of the beam was controlled by two adjustable apertures acting as spatial filters. The first aperture had a diameter of 7 mm and was located immediately after the laser. The second aperture, which had a diameter of 4 mm, was located in between the first polarizing beam splitter and the Faraday rotator.

Following the Faraday rotator, the beam passed through a half wave plate. This was added because some light was being transmitted back through the polarizing beam splitter, instead of being reflected, and is what caused the lens to be cracked in the beam minimizing system. When the adjustable apertures were put in instead of the lenses, the laser began popping on the first aperture. By placing the half wave plate after the Faraday rotator, the popping could be eliminated. Chapter 7 discusses this problem in more detail.

Next, the beam was spilt into two separate paths using the prism combination shown in Figure 5.1. Following this the beam was reflected at a $90^0$ angle off a high reflector, where it was either retro-reflected using another high reflector, or coupled into the fiber to produce SBS. A 10 cm focal length lens was used to couple the beams into the fiber. The reason for the $90^0$ reflection was to extend the distance from the prisms to the fiber in order to reduce the entrance angle of the beams. The beams are slightly apart from each other when leaving the prisms, and therefore are coupled into the fiber at a slight angle. To ensure both beams are coupled into the fiber, the entrance angle must be made smaller than the numerical aperture of the fiber (0.37). Figure 5.3 demonstrates this.

(a)                                    (b)
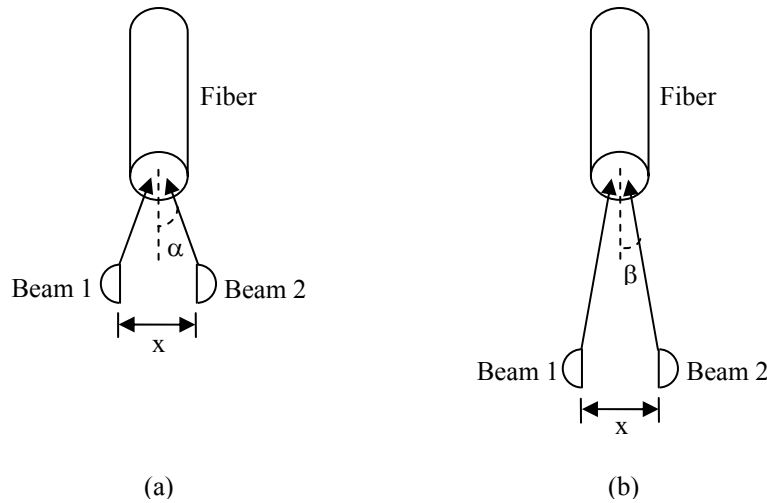
**Figure 5.3** Beam entrance angles into the fiber.

In both (a) and (b), the beams are separated by the same distance, x. The entrance angle, $\alpha$, in (a) is larger than the entrance angle, $\beta$, in (b), since the distance from the beam spots to the fiber is smaller in (a) than in (b).

For the case when the high reflector is used, the beam is retro-reflected back through the system until it reaches the polarizing beam splitter. At this point, the beam is reflected and passed through the same optical elements to reach the camera as in Figure 4.1. When the fiber is used instead of the high reflector, the return beam is the Stokes beam instead of a retro-reflection.

### 5.1.2.    Phasing Test without using the LSI

Since there was difficulty achieving usable LSI fringe data, another test was done to determine if phasing of the two beams took place. For the first part of the test, the set-up was the same as in Figure 5.2 with one exception. The LSI was taken out of the set-up, and the CCD camera was positioned so that it followed directly after the polarizing beam splitter. At this point the beams were checked to see if interference fringes were

formed as a result of phase differences between the two beams.  The presence of

interference fringes indicates a phase difference between the beams as a result of

traveling different paths through the prisms.  On the other hand, the absence of fringes

does not by itself prove that the beams are phased.  It must be shown that the SBS is

coherent after leaving the fiber.  Figure 5.4 shows the scheme that accomplished this.



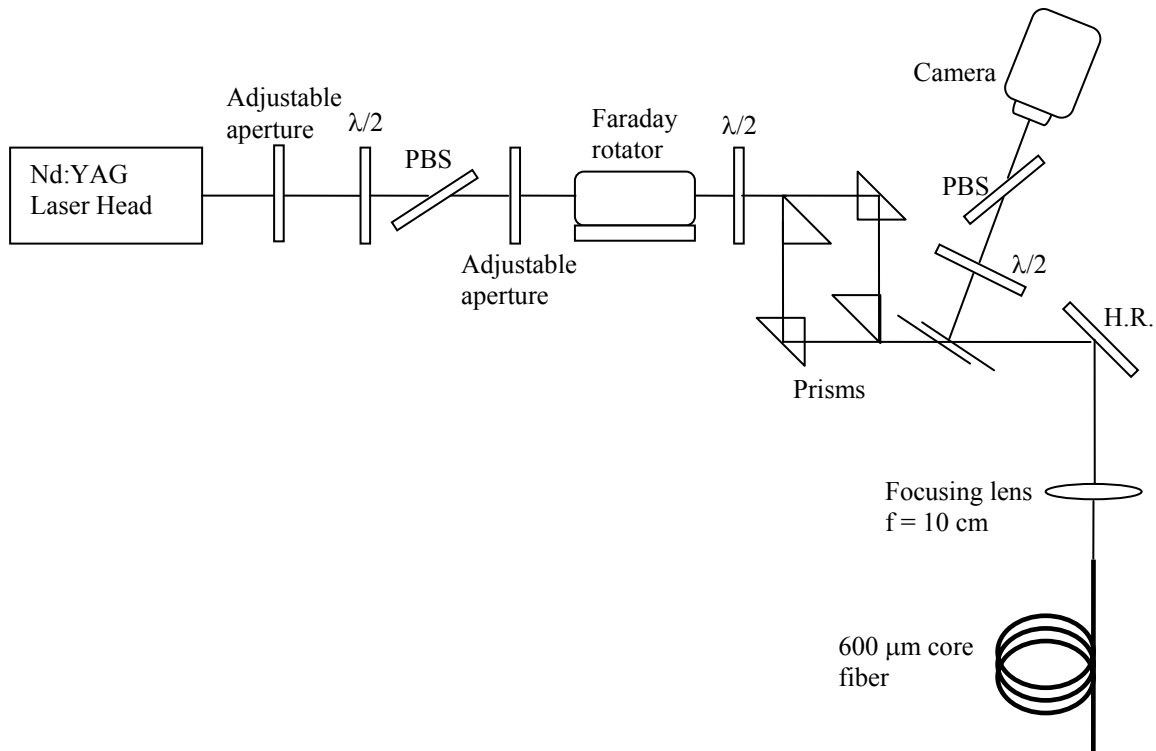**Figure 5.4** Set-up to determine if the SBS beams are coherent.

The set-up to test if the SBS beams are coherent is similar to that in Figure 5.2.  In

this case, the LSI is positioned between the prisms and the high reflector as shown in

Figure 5.4, and is used to overlap beam 1 and beam 2.  A small amount of the SBS

returning from the fiber is reflected off of each lateral shearing plate, and passed through

a half wave plate and polarizing beam splitter. As before, the half wave plate and

polarizing beam splitter are used to control the amount of light passed to the camera. The

reflections from the shearing plates are overlapped as shown in Figure 5.5. By adjusting

the lateral shearing plates, the reflections off each one can be oriented such that the beam

from one path through the prisms overlaps the beam from the other path through the

prisms. An indication of coherence is the formation of interference fringes.
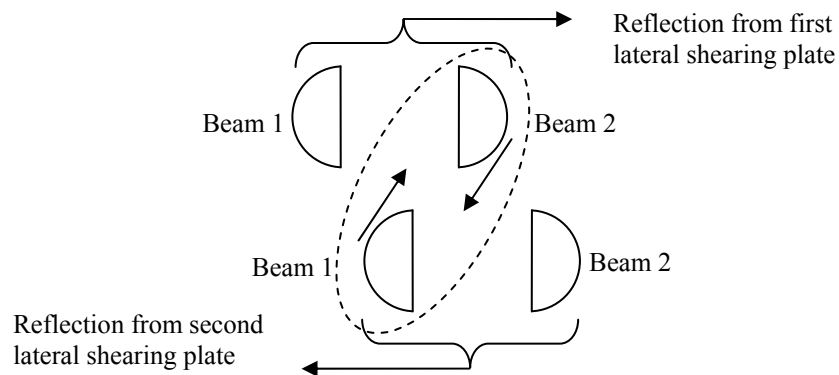


**Figure 5.5** Overlapping beam 1 and beam 2 to check for coherence.

By adjusting each lateral shearing plate, beam 2 from the first lateral shearing plate can be overlapped with
beam 1 from the second lateral shearing plate.

## *5.2.*     *Results*

As in the experimental procedures section, this section is divided into two parts

corresponding to the two different tests done.

## 5.2.1. Phasing Test using the LSI

As stated previously, using the LSI proved to be difficult in this test. The boundary regions were very difficult to determine. One of the possible reasons for this is the optics used for the lateral shearing plates. As explained in Appendix A, the lateral shearing plates were constructed from microscope slides. This allowed some reflection from the back surfaces of the slides which can interfere with the front surface reflections. Also, the microscope slides can add distortion since the surfaces are not as flat as would be desired. For more discussion on the LSI, see Appendix A.

Figure 5.6 shows a fringe pattern from the LSI when the fiber is used to get SBS. Both (a) and (b) are the same fringe pattern, with (b) having black lines drawn in where the boundaries are located.



<p style="text-align:center">(a)           (b)</p>

**Figure 5.6** Fringes from the LSI with the four prism set-up, using the fiber.

(a) The fringe pattern from the LSI when the beam is split into different optical paths using the four prisms. The fiber was used in this case to cause SBS. (b) The same fringe pattern as (a) with black lines drawn in over the boundary regions.

It is possible to determine where the boundaries are located by adjusting the location of the reflections from the different lateral shearing plates so that the two reflections are separated from each other. Then, as the reflections are brought together, the boundaries

can be identified. The figure also shows some distortion in the lower right corner of the pattern. This is a result of the poor quality of the microscope slides.

Figure 5.7 shows a fringe pattern for the case when the high reflector was used. Again, both (a) and (b) are the same fringe pattern with (b) having black lines drawn in over the boundaries. Comparing the fringe pattern in Figure 5.7 with the fringe pattern in Figure 5.6, it is seen that the continuity across the fringe boundaries in Figure 5.6 is broken in Figure 5.7. This indicates that the SBS beams from the fiber are phase, whereas the reflections from the mirror are not.



(a)                                                                                    (b)
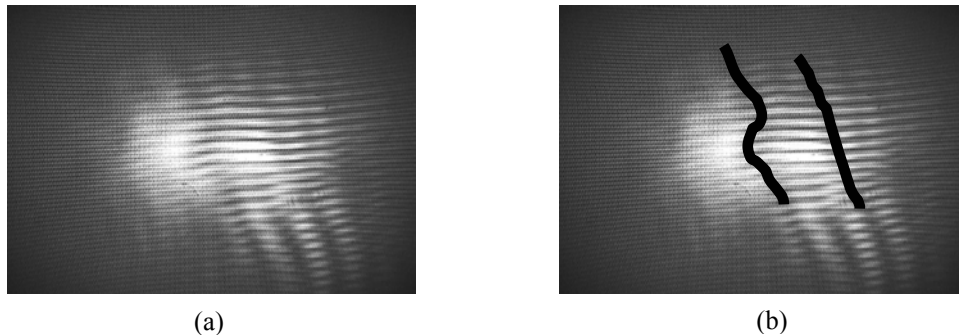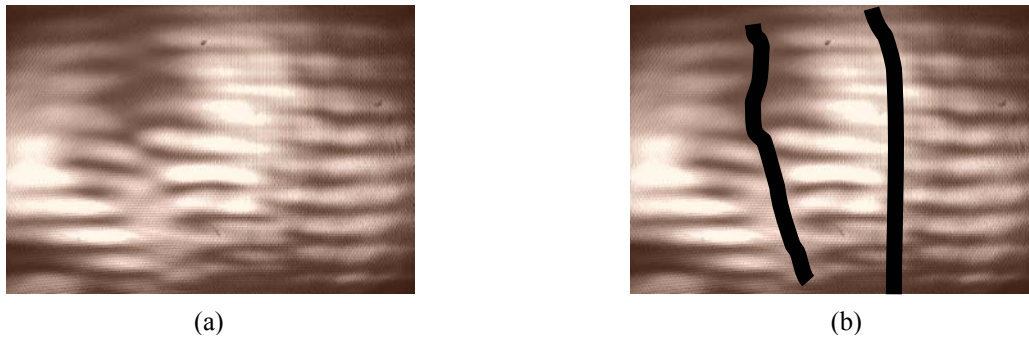
**Figure 5.7** Fringes from the LSI with the four prism set-up, using the high reflector.

(a) The fringe pattern from the LSI when the beam is split into different optical paths using the four prisms. The high reflector was used in this case as a retro-reflector. (b) The same fringe pattern as (a) with black lines drawn in over the boundary regions.

When the high reflector was used, it was possible to adjust the separation of the two separate beam paths at the LSI by slight adjustments to the prisms and the high reflector. Figure 5.8 demonstrates this. The figure shows a screen immediately after the return reflection from the polarizing beam splitter. Adjustment of prisms 1 and 2 control the location of beam 2, while prisms 3 and 4 control the location of beam 1. As beam 1 and beam 2 are brought close together, interference fringes form due to the phase

39

difference of the two different beams.  This proved to be a problem when the LSI was

used (the screen was removed) because in order to get the three interference regions from

the LSI, the beams needed to be brought close together, which in turn caused

interferences fringes to form before the LSI.  These interference fringes made it difficult

to distinguish the interference fringes formed by the LSI.  Therefore, it was difficult to

get meaningful interferograms from the LSI.  This problem did not arise when the fiber

was used instead of the high reflector since the SBS from the fiber was phase conjugated,

and adjustments of the prisms do not affect the location of the spots, as long as the beams

are still coupled into the fiber.
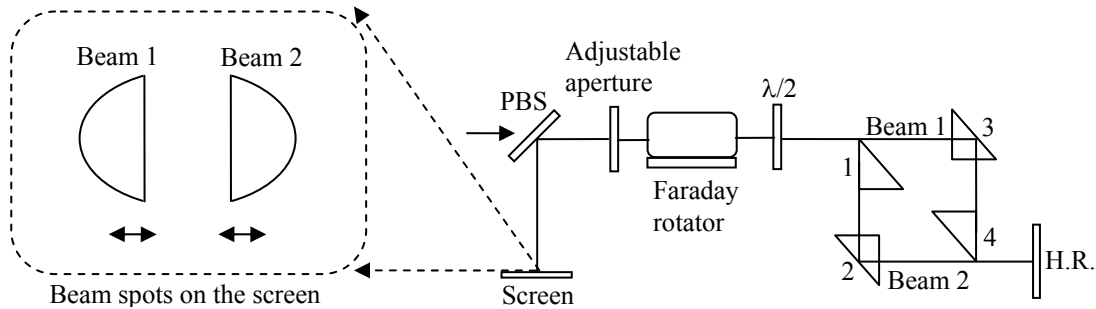


**Figure 5.8** Beam positioning using the prisms.

By adjusting prisms 1 and 2, the position of beam 2 on the screen can be controlled. Likewise, the position of beam 1 is controlled by prisms 3 and 4. When beams 1 and 2 are positioned too closely, interference fringes appear due to the phase difference of the beams.

### 5.2.2.        Phasing Test without the LSI

Since the interferograms from the LSI were somewhat ambiguous, additional tests

were conducted to determine if phasing of the two beams occurred.  As mentioned in the

experimental procedures section of this chapter, the LSI was replaced with the camera in

Figure 5.2 and the beams were checked to see if they formed interference fringes

40

together.  Figure 5.9 shows a comparison of the beam spots at the camera when the beam

is retro-reflected from the high reflector and when the fiber is used to produce SBS.  In

(a), the pattern resulting from the retro-reflection is seen.  When the beam spots are

brought together, as demonstrated by Figure 5.8, interference fringes are formed.  This

demonstrates the phase difference between the two beams.  In comparison, (b) shows the

spot pattern resulting from the SBS.  Here there are no interference fringes.  This by itself

is not enough to show that the beams have been phased.  It must also be shown that the

two beams are spatially coherent.  If the beams are not coherent, then fringes would not

be expected to be formed.



(a)                                                          (b)
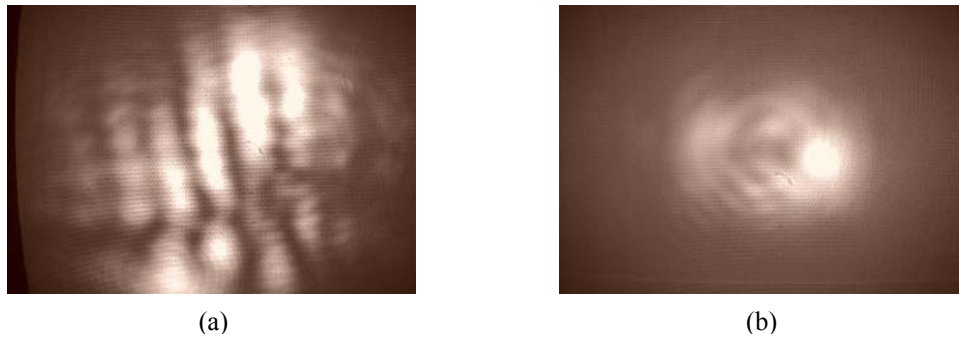
**Figure 5.9** Beam spot pictures to check for interference fringes.

(a) The beam spot picture taken of the return beam for the case when the high reflector is used.  The
presence of the interference fringes indicates that the two beams are not in phase. (b) The beam spot picture
of the return SBS beam for the case when the fiber is used. The absence of fringes is the first step in
concluding that phasing of the two beams has taken place. It must also be shown that the two beams are
coherent.

To this end, the final part of this test was to show that the two beams from the

SBS leaving the fiber were coherent.  Using the set-up shown in Figure 5.4, and the

method depicted in Figure 5.5, interference fringes were recorded at the camera.  Figure

5.10 shows the interference pattern observed.  The presence of these interference fringes

demonstrates that the Stokes beams exiting the fiber were coherent.

41

**Figure 5.10** Interference fringes from coherence test.

Since it was shown that the Stokes beams leaving the fiber were coherent by the presence of interference fringes when they overlappe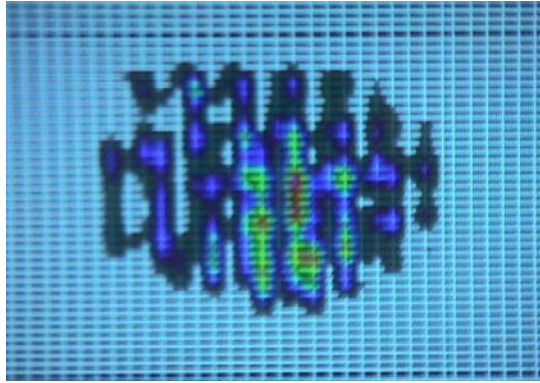d each other, the absence of fringes at the output now indicates the two beams were phased. Therefore, the phasing ability of the fiber in this set-up, where the beam wavefronts were spatially split by the prisms, was been demonstrated.

# 6 Characterization of SBS within the Fiber

This chapter discusses the temporal characteristics and energy of the Stokes beam. The SBS pulse width measurements were made simultaneously with pulse width measurements of the incident laser beam. In order to take these measurements, beam blocks were placed around the first polarizing beam splitter in Figure 5.2, such that they blocked the initial reflection of the laser beam and the reflection of the SBS beam. FND-100 detectors connected to a Lecroy 9450A, 300 MHz, digital oscilloscope were then used to record the pulse shape from the reflections off of the beam blocks. Figure 6.1 shows the placement of the beam blocks and detectors. Note that this does not include the entire set-up. Refer to Figure 5.2 for the set-up following the polarizing beam splitter.
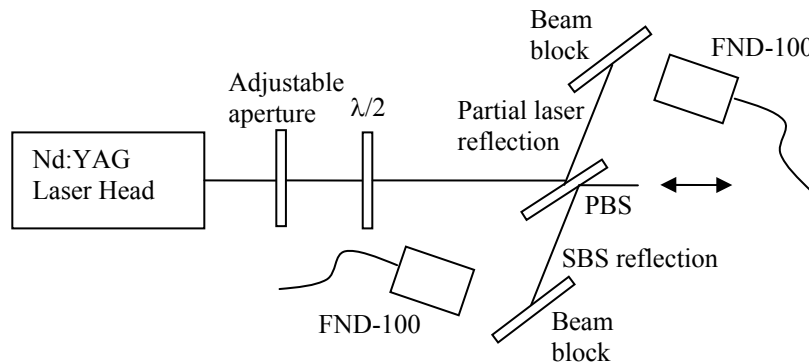


**Figure 6.1** Set-up to measure the pulse width of both beams.

The set-up following the polarizing beam splitter, denoted by the double arrow, is identical to that of Figure 5.2.

Figure 6.2 shows a comparison of both the pulse width of the laser and of the SBS. The average pulse width of the laser pulse was 15.3 ns, with a standard deviation of

0.6 ns.  In comparison, the average pulse width of the SBS pulse was 5.4 ns, with a standard deviation of 0.7 ns.
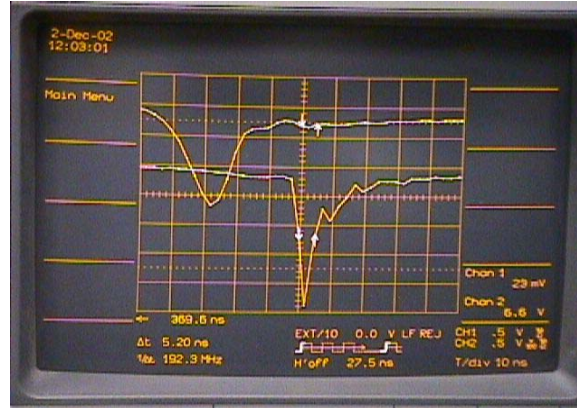


**Figure 6.2** Pulse width comparisons.
The wider pulse corresponds to the laser pulse, while the narrow pulse corresponds to the SBS pulse.

Figure 6.3 shows the set-up to measure the energy response of the SBS.  As in previous set-ups, the adjustable apertures control the beam diameter, the first half wave plate and polarizing beam splitter control the amount of light passed to the rest of the system, and the Faraday rotator rotates the beam by $45^0$ each time the light passes through it.  Also, as mentioned in Chapter 5, the half wave plate after the Faraday rotator is included to prevent the laser from popping on the first spatial filter.  See Chapter 7 for a discussion about this phenomenon.  Following the half wave plate, the beam is coupled into the fiber by a 10 cm focal length lens.  The 3.8 cm focal length lens following the fiber is used to focus the beam exiting the fiber, in order to take energy readings.  This was necessary due to the large divergence angle of the exiting beam.

**Figure 6.3** Set-up to measure the energy response of the SBS.

An energy meter was placed at positions 1-3. At position 1, the laser input energy was measured. The pump energy was measured at position2, and the SBS energy was measured at position 3.

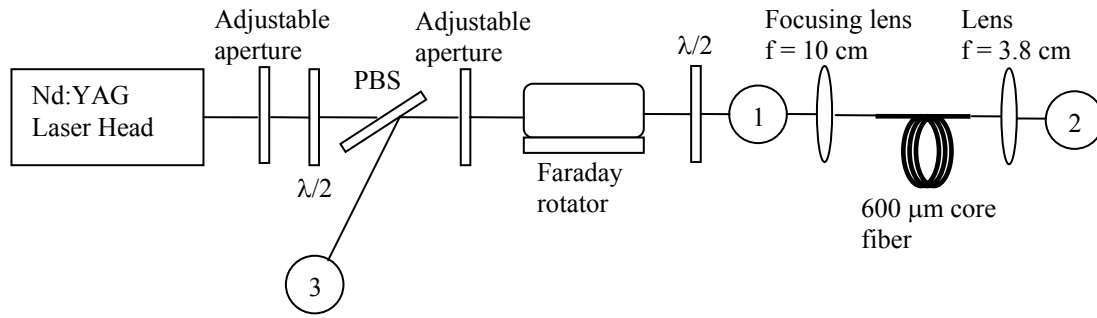Energy measurements were taken at three different locations in the set-up. The energy measurements taken at position 1 describe the energy of the laser prior to being coupled into the fiber. Measurements at position 2 describe the amount of the pump beam transmitted through the fiber. And finally, position 3 allowed energy measurement of the SBS to be taken. All the energy readings were taken as functions of the orientation of the first half wave plate. Figure 6.4 shows all three of the energies as the half wave plate is rotated to allow more light to be introduced to the fiber. This allows all three energies to be viewed against a common axis. The graph shows the pump depletion in comparison to the input energy as the threshold for SBS is reached and the SBS grows. Figure 6.5 plots the pump and SBS energies versus the input energy. Graphing the quantities in this manner gives insight into the distribution of the input beam between the pump and Stokes beam. It is seen that as the Stokes beam starts to grow, the transmitted pump beam energy starts to level off. In both Figure 6.4 and Figure 6.5, the pump energy is the pump energy transmitted through the fiber and recorded at position 2.
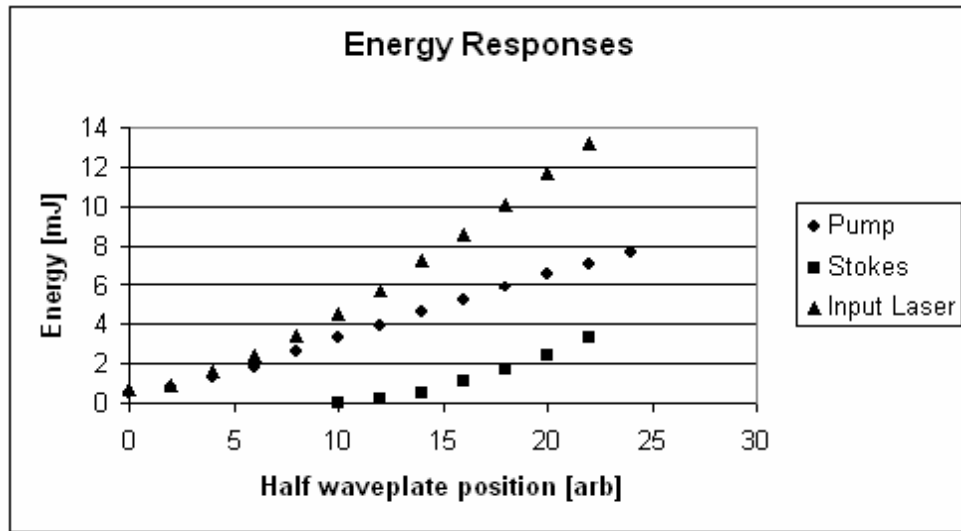
45

**Figure 6.4** Input energy, transmitted pump energy, and SBS energy responses.
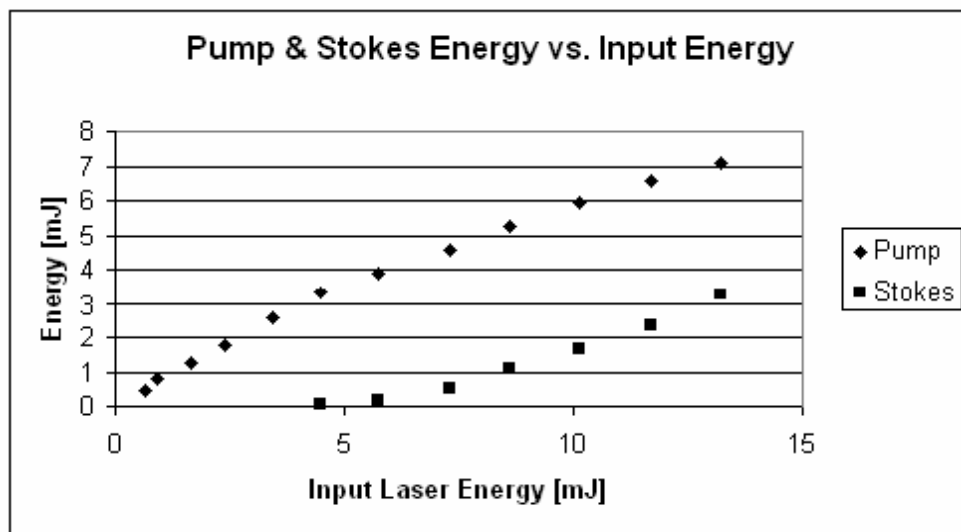


**Figure 6.5** Transmitted pump and SBS energy versus the input energy.

Beam coupling efficiency was determined by using the following relationship for the input energies below the SBS threshold.

$$E_o = \eta_c T_1 T_2 E_i \qquad\qquad (6.1)$$

where

$E_o$ = energy exiting the fiber and recorded at position 2

$E_i$ = energy input into the fiber recorded at position 1

$T_{1,2}$ = transmission at the corresponding fiber face

$\eta_c$ = beam coupling efficiency.

The values of $T_1$ and $T_2$ were 0.965, which corresponds to a Fresnel reflection of 3.5% at the entrance and exit fiber faces. Using Equation 6.1, the beam coupling efficiency is then

$$\eta_c = \frac{E_0}{T_1 T_2 E_i} . \qquad\qquad (6.2)$$

This method assumes a negligible attenuation within the fiber. In this manner, the coupling efficiency was found to be 82% with a standard deviation of 5%. The input energy level when SBS appeared was 4.5 mJ. Using a coupling efficiency of 82%, this translates to an SBS threshold of approximately 3.7 mJ.

The SBS slope efficiency was determined by calculating the slope of the SBS energy plotted against the input energy which is shown in Figure 6.5. The slope was found to be 0.37 which yields an SBS slope efficiency of 37%.

One of the difficulties in measuring the energy responses was to couple the beam into the fiber without damaging the fiber face. The fiber face has a low damage threshold, and is easily burned. Each time the fiber is damaged it must be re-cleaved and

47

polished to be used again.  The response for higher input energy proved to be difficult to achieve, due to the low damage threshold of the fiber.  This was the limiting factor for the graphs in Figure 6.4 and Figure 6.5.

# 7 Polarization Considerations

In Chapter 5, it was noted that the first lens in the beam minimizing system was damaged. Because of this, the beam minimizing system was removed from the set-up and replaced by a pair of adjustable apertures acting as spatial filters. This chapter details the experimental work and discovery of the damage to the beam minimizing lens. It was found that the Stokes beam was not completely linearly polarized like the pump beam was, and some of the beam was being transmitted back through the polarizing beam splitter into the laser. While a complete understanding of why the lens became cracked was not achieved, information about the Stokes beam polarization was investigated. The second half of this chapter discusses the results of the SBS generated Stokes beam polarization tests. The chapter ends with a brief discussion of how the prisms used in Chapter 5 to split the beam wavefronts may have generated elliptically polarized light.

## 7.1.  *Lens Damage Discovery*

The lens became damaged during the four prism beam splitting test. While trying to get phasing of the two beams using the SBS from the fiber, the first lens in the beam minimizing system cracked. In order to avoid damaging more lenses, the beam minimizing lenses were replaced with spatial filters (see Figure 5.2). At this point the half wave plate directly after the Faraday rotator was not part of the set-up. When the test began again, the laser began popping on the front side of the first aperture. In this case, the front side of the aperture is defined as the side facing the laser. It was found that the popping could be controlled by the first half wave plate. To determine if the popping had anything to do with the SBS, a beam block was placed immediately in front of the fiber.

With the beam block in place, no popping occurred regardless of the orientation of the half wave plate.

In an effort to stop the popping, another half-wave plate was added to the system and placed immediately after the Faraday rotator.  By adjusting the orientation of this half wave plate, the popping could be halted.  The four prism tests were then completed using this set-up.

## 7.2.        *SBS Polarization Investigation*

In trying to determine the cause of the damage to the lens, two questions needed to be investigated.  The first is the determination of the polarization state of the SBS. It is this topic that consumes the rest of this chapter.  The other question, which was not investigated, is how the beam was focused at the lens.  At this point, it appears that the focusing could have been caused by the SBS reentering the laser and having some interaction there.  This was not investigated, though, due to lack of time.

The first step in this investigation was to determine the polarization state of the beam prior to entering the fiber, and the polarization state of the returning SBS.  Figure 7.1 shows the set-ups for both of these tests.  In each case, the half wave plate and polarizing beam splitter are used to control the amount of light passed to the system, the adjustable apertures are used to spatially limit the beam diameter, and the first Glan polarizer is used to ensure the light passed to the Faraday rotator is linearly polarized. After passing through the Faraday rotator in (a), the beam passes another Glan polarizer and is terminated at an energy head.  By adjusting the second polarizer and taking energy readings, the polarization of the incident beam can be determined.

In (b), the beam passes through the Faraday rotator and a microscope slide at near normal incidence, where it is then coupled into the fiber using a 10 cm focal length lens. When the SBS passes back through the microscope slide, a small portion is reflected through a Glan polarizer and terminated at the energy head. Positioning the microscope slide at near normal incidence ensures the polarization state is not affected by the reflection. As in (a), the polarization can be determined by adjusting the second Glan polarizer and taking energy readings.
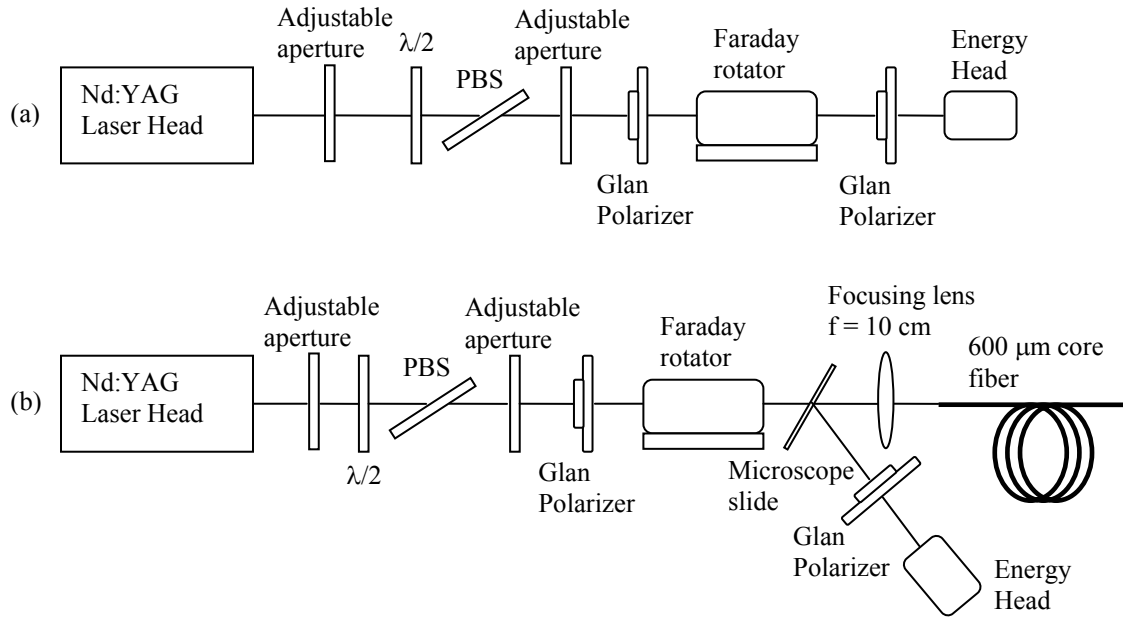


**Figure 7.1** Polarization test set-ups.

(a) The set-up to determine the polarization of the beam before it enters the fiber. (b) The set-up to determine the polarization of the SBS.

Figure 7.2 shows the energy readings for the incident beam, while Figure 7.3 shows the energy readings for the SBS beam. Each beam has a minimum located at $45^0$, but they do not both go to zero at this minimum. The beam that does go to zero is the incident beam. This indicates the beam is linearly polarized and oriented $45^0$ from the

vertical.  In comparison, the SBS beam does not go to zero at the $45^0$ minimum.  This is caused by one of two possibilities.  Either the beam is mostly linearly polarized at $45^0$ to the vertical with some random polarization, or the beam is slightly elliptical with its major axis oriented at $45^0$ to the vertical axis.



**Figure 7.2** Incident beam polarization test.

The energy in arbitrary units recorded as the polarizer in front of the energy head is rotated.
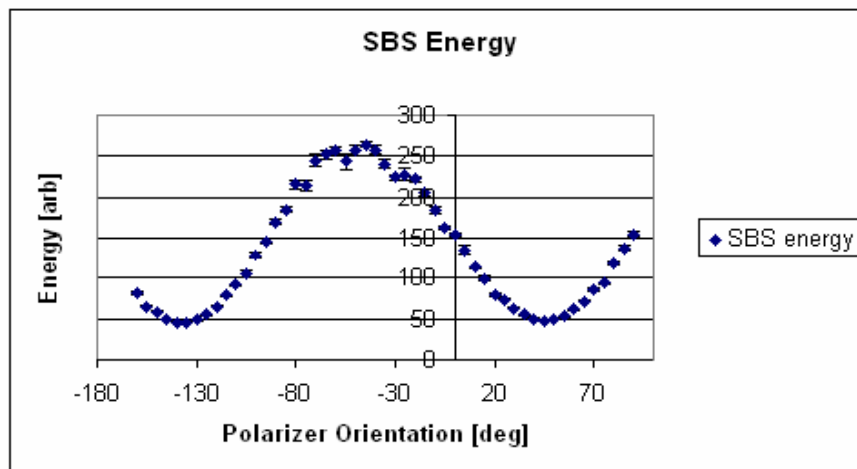


**Figure 7.3** SBS beam polarization test.
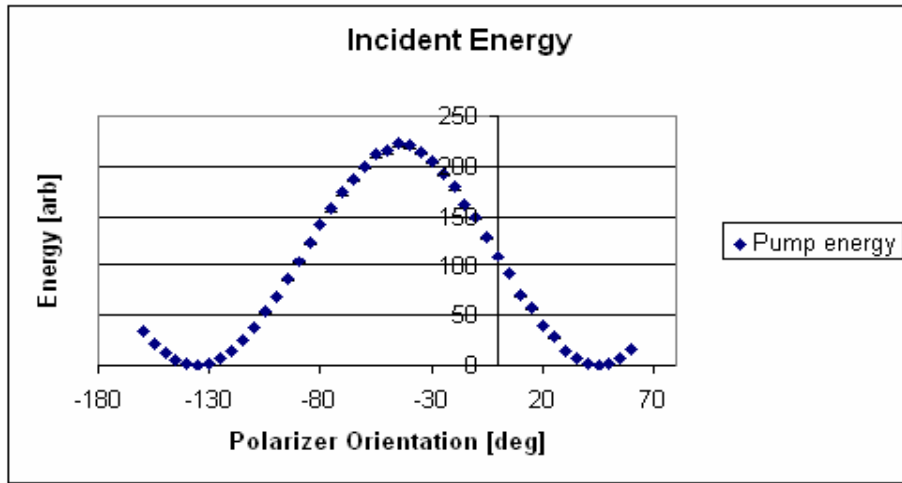
The energy in arbitrary units recorded as the polarizer in front of the energy head is rotated.

In order to determine whether the polarization of the SBS beam was slightly elliptical or slightly random, a quarter wave plate was placed before the second Glan polarizer. The fast axis of the quarter wave plate was aligned with the major axis of the beam polarization. If the beam polarization is elliptical, aligning the quarter wave plate in this manner would cause the beam to become linearly polarized, and the minimums of the energy readings as the Glan polarizer is rotated would go to zero. On the other hand, if the beam is slightly random, aligning the quarter wave plate in this fashion would have no effect on the energy readings. Figure 7.4 shows the energy readings as the polarizer was rotated.



**Figure 7.4** Random or elliptical SBS beam polarization test.

As seen in the figure, the minimums do not go to zero. This indicates the beam is linearly polarized with some random polarization. Unfortunately, during the course of

53

this particular test the laser began to exhibit trouble injection-locking, and there was not enough time to fix the problem before the al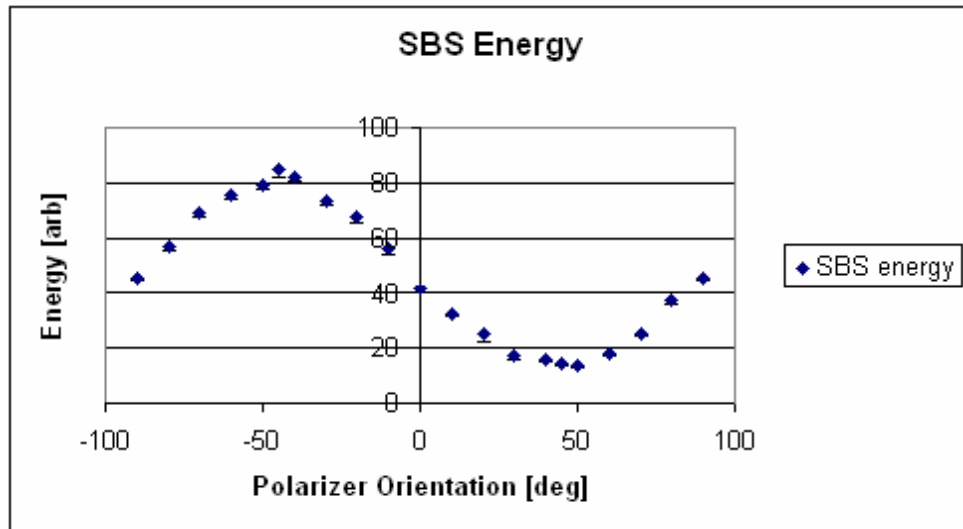lotted time for this project ran out. It would have been desirable to repeat this particular aspect of the polarization examination, but the problem with the laser prevented it. Therefore, the initial results indicate that the SBS generated Stokes beam is mostly linearly polarized with the same orientation as the pump beam, but has a small amount of random polarization.

The remainder of this chapter discusses a possibility of how the prisms that were used to create the separate optical paths in Chapter 5 could have effected the polarization of the beams. In Figure 5.2, after the beam exits the Faraday rotator in the forward direction, the beam is linearly polarized with its axis $45^0$ from both the vertical and horizontal axis. Without the half wave plate between the Faraday rotator and the first prism, the beam is incident on the prisms with both s- and p-polarization components. The total internal reflection that takes place within the prisms introduces a relative phase delay between the s and p components, and therefore the polarization becomes elliptical. Unless the SBS produces an exact phase conjugate of an elliptically polarized pump beam, the Stokes beam retracing the pump beam paths would not restore the linear polarization state of the pump beam. Hence, a finite fraction of the Stokes beam will be transmitted through the polarizing beam splitter into the laser system.

By placing a half-wave plate before the prisms, the pump beam polarization could be rotated such that it is entirely s- or p-polarized. This would ensure linear light is coupled into the fiber. This is a possible explanation of why the half wave plate controlled the amount of popping that occurred on the first aperture used to minimize the

beam diameter. This idea was not investigated due to time constraints and laser

difficulties, but is suggested for further work in this area.

# 8 Conclusion

The goal of this research was to determine the phasing properties of a short multimode optical fiber as a phase conjugate mirror in a system that handles multiple beams along separate optical paths. Two different situations were investigated in this project. The first was the case when separate optical paths were created by covering half of the laser beam with a microscope slide. The interferograms created by using a lateral shearing interferometer at the output beam demonstrated that the beams traveling the two optical paths were phased at the output of the system. The second was the case when separate optical paths were created using four prisms. A lateral shearing interferometer along with a CCD camera was used as the main diagnostic instrument for determining the phasing between the beams. In both cases investigated here, it was found that the fiber phase conjugator successfully phased the output beams.

The research described in this thesis provides a useful step forward to achieving an operational multi-channel double-pass MOPA system which utilizes an optical fiber as a phase conjugate mirror. Multi-channel MOPA systems are desirable in laser beam power scaling thanks to the use of multiple amplifiers instead of a single amplifier.

Previous research has shown that the piston errors can be reduced though SBS utilizing a bulk SBS medium as a phase conjugate mirror. Unfortunately, the systems are very sensitive to misalignment, and require the separate beams to be overlapped in a common focal volume within the medium.[3,5] As long as the beams are overlapped in a common focal volume, each beam will have the same absolute phase. On the other hand, if the beams are focused in different focal volumes, they will have a random absolute phase difference relative to each other, and therefore no phasing will occur. The

advantage of using optical fibers as the phase conjugate mirror is that the misalignment problems of the SBS cell are largely eliminated. The fiber confines the beams to its core, which ensures the beams overlap over a long interaction length. This in turn means the Stokes beams that are produced have the same phase. Present research clearly demonstrated that a short multimode optical fiber used as a phase conjugate mirror can phase the beams that traveled through two separate optical paths.

In this research, a Q-switched laser with a pulse width of approximately 15 ns was used as the pump beam. This led to one of the difficulties encountered during the investigations. Since the Q-switched pulses are so short, they lead to pump pulses with very high peak power. This in turn makes coupling the pump beam into the fiber without damaging the fiber face difficult. In fact, the damage threshold of the fiber was the limiting factor for the amount of energy that could be coupled into the fiber.

In a practical application of this research, a continuous wave (cw) pump or a non Q-switched pulsed pump could be used to couple more energy into the fiber. The peak power of such a pump beam would be much less than for the Q-switched pump, and therefore would allow more energy to be coupled into the fiber before the damage threshold of the fiber was reached. In addition to the energy benefits, a longer pulse or a cw pulse would be expected to produce a much higher overall SBS efficiency.

When perfected, it is possible that this technology could produce a high power output laser beam using a much lower power laser source. For example, it could be possible to achieve a 1 kilowatt class cw laser using a 100 watt class laser in a MOPA configuration with 10 to 15 channels. This would make many low power laser systems possible candidate lasers for applications such as electronic countermeasures.

There are many areas in which to extend the investigations done in this project. First, more optical paths should be incorporated into the system, allowing the fiber to be tested for phasing of more than two beams traveling separate optical paths. Also, the phasing properties of the fiber should be investigated when real optical amplifiers are placed within the separate optical paths. Another area of interest is the polarization properties of both the prisms and the SBS on the beam. In particular, the polarization state of the Stokes beams need to be re-examined and the mechanisms responsible for the lens damage needs to be identified and measures taken to prevent the damage. Finally, quantified measurements need to be performed to identify the phasing efficiency of the beams.

# Appendix A: Lateral Shearing Interferometer

Figure A.1 shows the schematic for the lateral shearing interferometer (LSI).
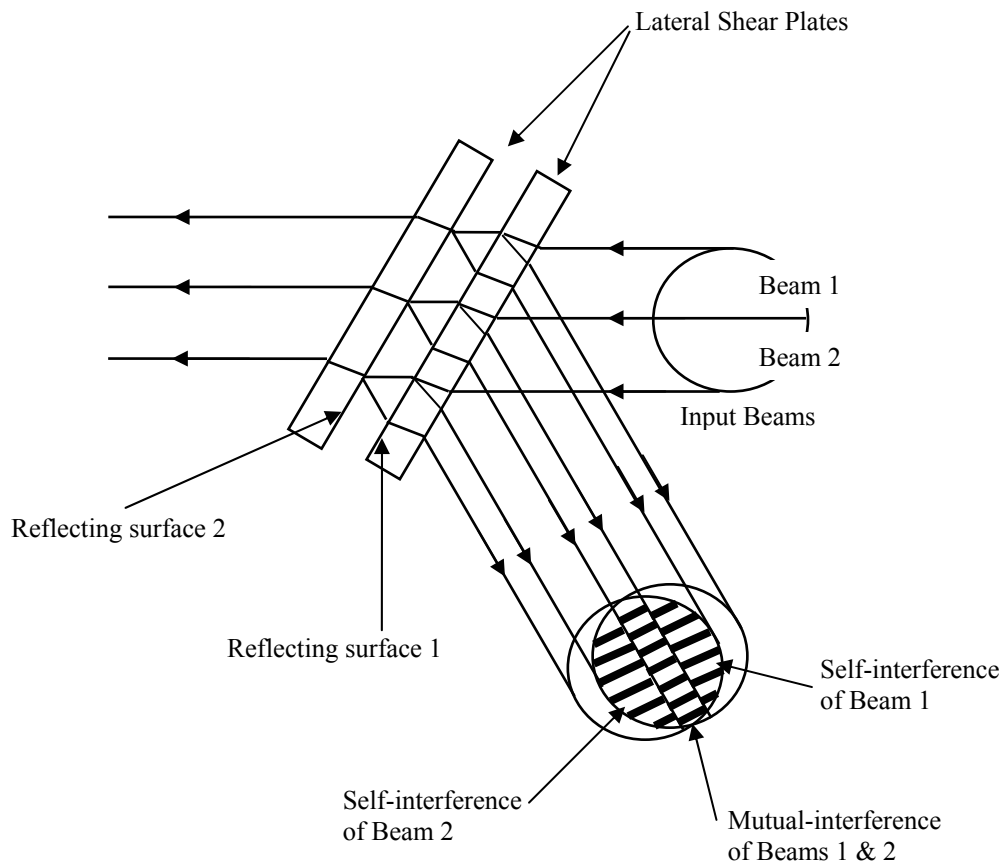


**Figure A.1** Lateral shearing interferometer.

The purpose of the LSI is to create an interferogram using the reflections from the front

surface of each plate to determine the phase relationship between the two beams. In this

project the LSI was constructed of two uncoated microscope slides. Each slide was held

by a prism mount attached to a one dimensional translation stage. This allowed for

independent tilt, rotation, and translation of each slide. Ideally, optical wedges are the

best choice for the lateral shear plates, since the reflections from the back surfaces of the

plates will not be reflected in the same direction as the front surface reflections. Optical wedges were not available in a suitable time frame for this project, so the microscope slides were used instead.

As stated previously, the operating principle of the LSI is based on the interference patterns generated by the overlap of the reflections from the front surface of each lateral shear plate. The beams from each of the separate optical paths are incident on the lateral shear plates, where each is reflected as shown in Figure A1. The reflection of beam 1 from the surface of the second plate overlaps the reflections of both beam 1 and beam 2 from the first plate. At the same time, the reflection of beam 2 from the second plate overlaps the reflection of beam 2 from the front plate. This creates three regions of interference fringes. On one side is the self interference of beam 1 with itself, while on the other side is the self interference of beam 2 with itself. In between these regions is a region of mutual interference of beam 1 and beam 2. If the fringes are continuous across the three regions, then there is conjugation (phasing) of the relative piston error between the two beams.

# Bibliography

1. P. M. Fishbane, S. Gasiorowicz, and S.T. Thortin, *Physics for Scientists and Engineers*, 2 ed. New Jersey: Prentice-Hall Inc., 1996.

2. S. Gourley, "Making Light Legal," *Jane's Defense Weekly*, vol. 33, pp. 22-26, 2000.

3. R. H. Moyer, M. Valley, and M.C. Cimolino, "Beam combination through stimulated Brillouin scattering," *J. Opt. Soc. Am. B*, vol. 5, pp. 2473-2489, 1988.

4. B. Ya. Zel'dovich, V.I. Popovichev, V.V. Ragul'skii, and F.S. Faisullov, "Connection between the wave fronts of the reflected and exiting light in stimulated Mandel'shtam-Brillouin scattering," Pis'ma Zh. Eksp. Teor. Fiz. 15, 160-164 (1972) [JTEP Lett. 15, 109-113 (1972)].

5. S. Sternklar, D. Chomsky, S. Jackel, and A. Zigler, "Misalignment sensitivity of beam combining by stimulated Brillouin scattering," *Opt. Lett.*, vol. 15, no. 9, pp. 469-470, May 1990.

6. B. C. Rodgers, T. H. Russell, and W. B. Roh, "Laser beam combining and cleanup by stimulated Brillioun scattering in a multimode optical fiber," *Optics Lett.*, vol. 24, no. 16, pp. 1124-1126, August 1999.

7. M. Gower, D. Proch, *Optical Phase Conjugation*, Berlin: Springer-Verlag, pp. 74-96, 1994.

8. R. A. Fisher, *Optical Phase Conjugation*, New York: Academic Press Inc., pp. 2-15, 1983.

9. D. M. Pepper, "Nonlinear optical phase conjugation," *Optical Engineering*, vol. 21, no. 2, pp. 156-183, March/April 1982.

10. J. Sakai, *Phase Conjugate Optics*, New York: McGraw-Hill, pp. 5-8, 1992.

11. G. S. He, S. H. Liu, *Physics of Nonlinear Optics*, New Jersey: World Scientific Publishing Co. Pte. Ltd., 1999.

12. G. P. Agrawal, *Nonlinear Fiber Optics*, San Diego: Academic Press Inc., 1989.

13. R. W. Boyd, *Nonlinear Optics*, San Diego: Academic Press Inc., 1992.

14. N. G. Basov, I. G. Zubarev, A. B. Mironov, S. I. Mikhailov, and A. Y. Okulov, "Laser interferometer with wavefront-reversing mirrors," Zh. Eksp. Teor. Fiz. 79, 1678-1686, 1980 [Sov. Phys., JETP 52, 847-851 (1980)].

15. M. Valley, G. Lombardi, and R. Aprahamian, "Beam combination by stimulated Brillouin scattering," *J. Opt, Soc. Am. B*, vol. 3, no. 10, October 1986.

16. B. Ya. Zel'dovich, V. V. Shkunov: Kvant. Electron. 4, 1090-1098, 1977 [Sov. J. Quantum Electron. 4, 610 (1977)].

# Vita

Second Lieutenant Shawn M. Willis graduated from Gem State Academy High School in Caldwell, Idaho. He enlisted in the United States Air Force in December 1992. After technical training as a precision measurement equipment laboratory (PMEL) specialist, he was assigned to the 366th Maintenance Squadron, Mountain Home AFB, Idaho where he served as a PMEL technician. In March 1994, he was assigned to the 15th Maintenance Squadron, Hickam AFB, Hawaii where he served as a PMEL technician.

In August 1997, he was released from active duty to attend the University of Idaho in Moscow, Idaho where he graduated Summa Cum Laude with a Bachelor of Science degree in Physics in May 2002. He was commissioned through the Detachment 905 AFROTC at Washington State University where he was recognized as a Distinguished Graduate. His first commissioned assignment, in August 2002, was at the Graduate School of Engineering and Management, Air Force Institute of Technology, Wright-Patterson AFB, Ohio where he pursued a Master of Science degree in Physics.

## REPORT DOCUMENTATION PAGE

*Form Approved*
*OMB No. 074-0188*

The public reporting burden for this collection of information is estimated to average 1 hour per response, including the time for reviewing instructions, searching existing data sources, gathering and maintaining the data needed, and completing and reviewing the collection of information. Send comments regarding this burden estimate or any other aspect of the collection of information, including suggestions for reducing this burden to Department of Defense, Washington Headquarters Services, Directorate for Information Operations and Reports (0704-0188), 1215 Jefferson Davis Highway, Suite 1204, Arlington, VA 22202-4302. Respondents should be aware that notwithstanding any other provision of law, no person shall be subject to an penalty for failing to comply with a collection of information if it does not display a currently valid OMB control number.
**PLEASE DO NOT RETURN YOUR FORM TO THE ABOVE ADDRESS.**

| 1. REPORT DATE (DD-MM-YYYY) 03-03-2002 | 2. REPORT TYPE **Master's Thesis** | 3. DATES COVERED (From – To) Oct 2002 – Mar 2003 |
|---|---|---|

**4. TITLE AND SUBTITLE**

Phasing a Dual Optical Path System Using an Optical Fiber as a Phase Conjugate Mirror

**5a. CONTRACT NUMBER**

**5b. GRANT NUMBER**

**5c. PROGRAM ELEMENT NUMBER**

**6. AUTHOR(S)**

Willis, Shawn, M., 2 Lt, USAF

**5d. PROJECT NUMBER**
02-265

**5e. TASK NUMBER**

**5f. WORK UNIT NUMBER**

**7. PERFORMING ORGANIZATION NAMES(S) AND ADDRESS(S)**
Air Force Institute of Technology
Graduate School of Engineering and Management (AFIT/EN)
2950 P Street, Building 640
WPAFB OH 45433-7765

**8. PERFORMING ORGANIZATION REPORT NUMBER**

AFIT/GAP/ENP/03-06

**9. SPONSORING/MONITORING AGENCY NAME(S) AND ADDRESS(ES)**
Howard Schlossberg
AFOSR/NE
Air Force Office of Scientific Research
801 North Randolph Street Rm 732
Arlington, VA 22203

**10. SPONSOR/MONITOR'S ACRONYM(S)**

**11. SPONSOR/MONITOR'S REPORT NUMBER(S)**

**12. DISTRIBUTION/AVAILABILITY STATEMENT**

APPROVED FOR PUBLIC RELEASE; DISTRIBUTION UNLIMITED.

**13. SUPPLEMENTARY NOTES**

**14. ABSTRACT**
Phase conjugation properties of stimulated Brillouin scattering (SBS) in a short multimode fiber have been investigated with an eye towards its application for a multi-channel double pass master oscillator power amplifier (MOPA) system. In particular, properties of the SBS beam to compensate for the axial and transverse phase distortion between individual channels in a multi-channel amplifier system were studied. Two optical paths were created by covering half of the laser beam with a microscope slide, and also by spatially splitting the wavefronts with a 4 prism set-up. The Stokes beams that traversed the same optical paths as the pump beams were shown to compensate the phase distortion introduced by the different optical paths.

**15. SUBJECT TERMS**
Lasers, Optics, Fiber Optics, Nonlinear Optics, Phase Conjugation, Brillioun Scattering, Stokes Radiation, Interference Fringes, Phasing

| 16. SECURITY CLASSIFICATION OF: | | | 17. LIMITATION OF ABSTRACT | 18. NUMBER OF PAGES | 19a. NAME OF RESPONSIBLE PERSON Won B. Roh, AFIT/ENP |
|---|---|---|---|---|---|
| a. REPORT U | b. ABSTRACT U | c. THIS PAGE U | UU | 73 | 19b. TELEPHONE NUMBER (Include area code) (937) 255-3636, ext 4509 |

**Standard Form 298 (Rev. 8-98)**
Prescribed by ANSI Std. Z39-18